

GENERAL CIRCULATION OF JUPITER'S ATMOSPHERE

Francis Rust Wooldridge

Library
School Postgraduate School
Palo Alto, California 93940

NAVAL POSTGRADUATE SCHOOL

Monterey, California



THESIS

GENERAL CIRCULATION OF JUPITER'S ATMOSPHERE

by

Francis Rust Wooldridge

Thesis Advisor:

R. T. Williams

March 1973

T 154596

Approved for public release; distribution unlimited.

General Circulation of Jupiter's Atmosphere

by

Francis Rust Wooldridge
Lieutenant, United States Navy
B.S., Virginia Polytechnic Institute, 1967

Submitted in partial fulfillment of the
requirements for the degree of

MASTER OF SCIENCE IN METEOROLOGY

from the

NAVAL POSTGRADUATE SCHOOL
March 1973

ABSTRACT

A three-level quasi-geostrophic atmospheric model on a mid-latitude β -plane with a single wave in the x-direction and a thick lower layer was developed. This model was used to determine the disturbance structure in y for linear interactions with a constant mean wind and nonlinear interactions with a varying mean wind. Simple heating to maintain the mean wind and friction were included in the nonlinear case.

The linear experiment produced exponential growth rates in the disturbance field that were independent of the lower layer thickness. These waves were baroclinically unstable. The mean wind field showed large modifications for a Rossby deformation length of 75 KM at 10^4 Jupiter days.

TABLE OF CONTENTS

I.	INTRODUCTION -----	5
II.	THE MODEL AND FORECAST EQUATIONS -----	10
	A. DESCRIPTION -----	10
	B. METHOD OF SOLUTION -----	11
III.	RESULTS -----	24
IV.	CONCLUSIONS -----	51
	APPENDIX -----	53
	LIST OF REFERENCES -----	55
	INITIAL DISTRIBUTION LIST -----	57
	FORM DD 1473 -----	62

ACKNOWLEDGEMENTS

The author wishes to express his deep gratitude to Dr. Roger Terry Williams whose recommendations, counsel, encouragement, and great patience not only made this thesis possible, but also provide me with the desire to complete my studies.

I would further like to thank Dr. Robert L. Haney for his suggestions and discussions which contributed to this study. Thanks is offered to the W. R. Church computer center personnel who have provided me with the computer services required for this project in a truly outstanding manner.

Finally, I want to thank my wife, Joyce, whose quiet understanding and devotion made this effort possible.

I. INTRODUCTION

The meridional belts (dark bands) and zones (light bands) of Jupiter have been recorded since this planet was first observed through a telescope. The features found in these regions are semi-permanent and have a variety of rotation rates. Peek (1958) assembled this information to show the variation of zonal velocity with Jovian latitude. Evidence was found by Chapman (1969) for anticyclonic shear to be associated with the zones and for cyclonic shear to be associated with the belts, but the correlation was imperfect.

Ingersoll and Cuzzi (1969) have investigated the barotropic instability of the observed motions at mid-latitudes using data from Peek (1958). Geostrophic balance and symmetric temperature difference between the belts and zones were assumed. The validity of the assumptions was verified by the excellent agreement between predicted and observed zonal velocities. It was also shown that the relative vorticity gradient U'' approaches, but does not exceed the planetary vorticity gradient β . This is the necessary condition for barotropic instability. Thus barotropic instability probably limits either the belt wave number or the amplitude of the zonal flow. It was further shown that the zones are warmer than the belts.

Stone (1967) applied the baroclinic stability theory to the dynamics of the Jovian atmosphere. He tested the

hypothesis that the zonal motions in Jupiter's atmosphere are thermal winds and that the latitudinal cloud bands are caused by baroclinic instabilities under non-geostrophic conditions. Stone (1966a) showed that at least three different kinds of baroclinic instability can occur when $d\theta/dZ > 0$. The kind of instability that dominates depends upon the value of the non-dimensional Richardson number

$$Ri = \frac{g}{\theta} \frac{\partial \theta}{\partial Z} / \left(\frac{\partial U}{\partial Z} \right)^2, \quad (1.1)$$

where g is the acceleration of gravity, θ is the potential temperature, $\frac{1}{\theta} \frac{\partial \theta}{\partial Z}$ is a representative vertical stability, and $\frac{\partial U}{\partial Z}$ a characteristic vertical shear of the wind. The Richardson number is a characteristic ratio of work done against gravitational stability to energy transferred from mean to turbulent motion. He assumed that the observed winds on Jupiter are due to symmetrical instabilities with no longitudinal variations. This type of instability dominates in the range $0.25 < Ri < 0.95$. Allowance for a deep atmosphere was made by not using the Boussinesq approximation for compressibility. It was shown that in a deep atmosphere symmetric instabilities form in the specified range of Ri and that these instabilities may extend over many scale heights. Thus the zonal winds and the latitudinal cloud bands may be explained qualitatively by assuming the presence of north-south temperature gradients caused by differential solar heating. These gradients will drive thermal winds in

the zonal direction, and under appropriate conditions, symmetric instabilities can grow, generating latitudinal cloud bands.

Gierasch, Ingersoll, and Williams (1973) demonstrated that a cloudy planetary atmosphere at rest is unstable to disturbances of large horizontal scale. The energy source for this instability is the change in radiative heat flux associated with a vertical displacement near the emitting level. The important feature of the model was that the net heating rate Q is proportional to the vertical displacement δZ of the cloud from its equilibrium position. Quasi-steady geostrophic motions or short period oscillations, representing inertia-gravity waves may become unstable in the presence of radiative heating. Gierasch and Goady (1969) found that the radiative time constants of Jupiter are longer than the dynamical time constants in the earth's atmosphere; therefore, the geostrophic mode was applied, since the instability can be quasi-geostrophic. Gierasch, Ingersoll, and Williams (1973) derived a value of 19,000 KM for the y-scale wavelength at 23° latitude which corresponds to the limiting amplitude for an axisymmetric geostrophic instability where the wave-number in the x-direction $k_x = 0$. This y-length is essentially equal to the observed belt-zone pair at this latitude. They also computed the value of the radiative time constant λ_c^{-1} . For an isothermal atmosphere λ_c^{-1} was approximately equal to 160 years. It was also observed that even if the lapse rate differed from the adiabatic lapse rate by only

1%, the radiative time constant would be about 1.6 years. These results are consistent with the observed lifetimes of atmospheric features on Jupiter.

Gierasch (1973) studied the radiative instability of a cloud deck on an equatorial β -plane as discussed by Gierasch, Ingersoll, and Williams (1973). The model was based on the assumption that a precipitating condensable atmospheric constituent can be concentrated in the atmosphere by vertical motion. If the condensing constituent is radiatively important, it can cause radiative warming at the locations where it is concentrated. As a result, the heating is related to vertical motion and reinforcement is possible. They considered two values of the Rossby deformation length

$$Ri = \sqrt{\frac{g'H}{f}}, \quad (1.2)$$

where g' is reduced gravity, f is the Coriolis parameter, and H is a characteristic height. Static stability estimates by Lewis (1969) and Stone (1972) gave characteristic lengths of 785 KM and 78.5 KM, respectively. It was concluded that the radiative instability mechanism driven by the dynamical concentration of a condensable constituent, produces instabilities with the wavelength and zonal symmetry of Jupiter's bands. Nonsymmetric instabilities with a shorter wavelength also exist. Finally, the structure of

the modes is in agreement with Ingersoll and Cuzzi's (1969) conclusion that cloudy zones are warmer than belts.

A three-level quasi-geostrophic model incorporating a deep lower layer, as suggested by Gierasch (1973), was developed based on the Charney and Phillips (1953) multi-level model. The model was modified by implementing Lorenz's (1960) technique of replacing the dependent variable with Fourier coefficients.

The objective of this study was to define the linear disturbance structure in y and to see if the belt-zone wind growth rate due to quasi-geostrophic baroclinic instability decreases with greater lower layer depth. Non-linear interactions with the belt-zone flow pattern were then studied incorporating simple heating, to maintain the zonal winds, and friction. These objectives were evaluated using two values for the Rossby deformation length.

II. THE MODEL AND FORECAST EQUATIONS

A. DESCRIPTION

The atmospheric model for these experiments was based on the quasi-geostrophic equations. The model was constructed on a β -plane with a central latitude of 45 degrees. Since the large-scale motions in the extra-tropical latitudes of Jupiter are quasi-geostrophic, the domain of the model was restricted to the middle latitudes. Phillips (1963) discussed geostrophic motions with approximately uniform potential vorticity. These motions have characteristic wavelengths of about 4,000 KM on earth, or the order of the Rossby deformation length. He used an expansion in the Rossby number, $R_0 = U/fL$, where U is a characteristic velocity, f is the Coriolis parameter, and L a characteristic length. This expansion showed that the β -plane approximation is justified for geostrophic motions of this type. Gierasch, Ingersoll, and Williams (1973) have shown that large-scale bands have a characteristic scale of 15,000 KM in the atmosphere of Jupiter. It was further shown that the Rossby number R_0 is much less than one. If the rotation is sufficiently fast such that R_0 is of order one or less, Coriolis forces become important and must be considered in the equations of motion. The additional conditions of R_L/a , where a is the planetary radius, being small, and the large-scale waves being greater than or equal to R_L are

satisfied; therefore, the geostrophic assumption is valid. The geophysical constants for earth and Jupiter are summarized in the appendix.

A three-level model was developed so that heating and friction could be included and still satisfy the lower boundary condition. Since the interior of the planet is not known, a deep lower layer is used to remove the two upper layers from the lower boundary. The solution function and its derivatives were forced to vanish at the boundaries. The Jovian atmosphere was divided into six layers numbered 1 through 6 as shown in Figure 1. The upper layers, 0-4, have thickness $\Delta P/2$; and the lower layers, 5 and 6, have thickness $P/2$, where $P \gg \Delta P$ in this application. The thickness between levels 3 and 5 is defined to be $\pi = (\Delta P + P)/2$. In general these thickness relationships are arbitrary.

B. METHOD OF SOLUTION

The quasi-geostrophic vorticity equation on a β -plane is

$$\frac{\partial \zeta}{\partial t} + \mathbf{V} \cdot \nabla (\zeta + \beta_0 y) - f_0 \frac{\partial \omega}{\partial P} = B \nabla^2 \zeta , \quad (2.1)$$

$$\text{where } \zeta = \frac{1}{f_0} \nabla^2 \phi , \quad \mathbf{V} = \frac{1}{f_0} \mathbf{k} \times \nabla \phi , \quad (2.2)$$

and the thermodynamic equation is

$$\frac{\partial}{\partial t} \frac{\partial \phi}{\partial P} + \mathbf{V} \cdot \nabla \frac{\partial \phi}{\partial P} + \omega \sigma = \frac{1}{\tau} \left(\frac{\partial \phi^*}{\partial P} - \frac{\partial \phi}{\partial P} \right) , \quad (2.3)$$

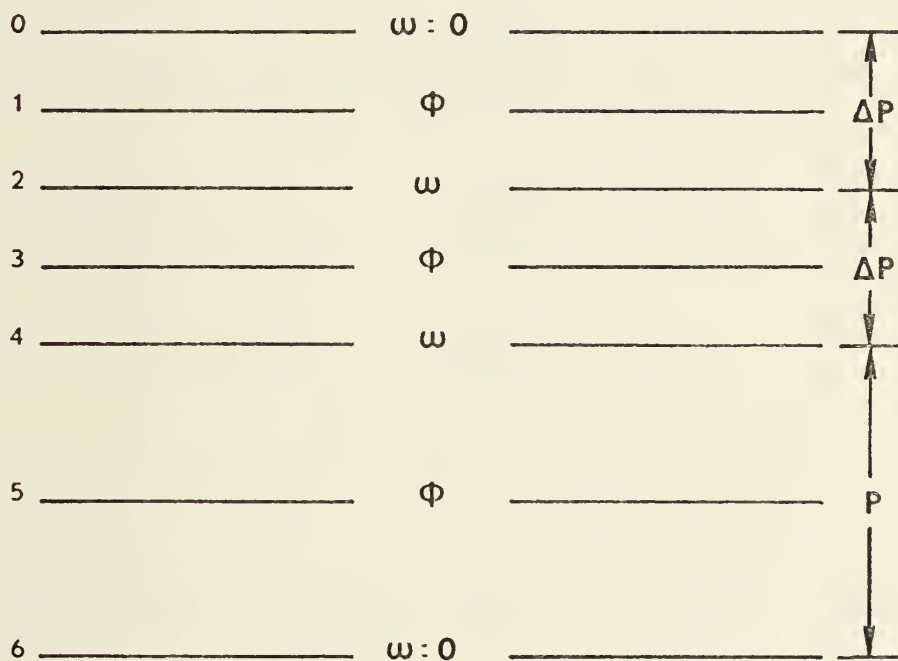


FIGURE 1 - The Three-Level Model
Variables are evaluated at the layers shown.

where $\omega = \frac{dP}{dt}$ and σ is defined as the static stability. The quantity τ is the radiative time constant and $\frac{\partial \phi^*}{\partial P}$ is an equilibrium temperature which is dependent upon radiation, convection, and other small scale parameters. Equation (2.1) was applied at levels 1, 3, and 5 which yielded

$$\frac{\partial \zeta_1}{\partial t} + V_1 \cdot \nabla (\zeta_1 + \beta_0 y) - f_0 \frac{\omega_2 - \omega_0}{P_2 - P_0} = BV^2 \zeta_4 \quad , \quad (2.4)$$

$$\frac{\partial \zeta_3}{\partial t} + V_3 \cdot \nabla (\zeta_3 + \beta_0 y) - f_0 \frac{\omega_4 - \omega_2}{P_4 - P_2} = BV^2 \zeta_3 \quad , \quad (2.5)$$

$$\frac{\partial \zeta_5}{\partial t} + V_5 \cdot \nabla (\zeta_5 + \beta_0 y) - f_0 \frac{\omega_6 - \omega_4}{P_6 - P_4} = BV^2 \zeta_5 \quad , \quad (2.6)$$

Equation (2.3) applied to levels 2 and 4 yielded

$$\frac{\partial}{\partial t} \left(\frac{\phi_3 - \phi_1}{P_3 - P_1} \right) + V_2 \cdot \nabla \left(\frac{\phi_3 - \phi_1}{P_3 - P_1} \right) + \sigma_2 \omega_2 = \frac{1}{\tau} \left[\left(\frac{\partial \phi^*}{\partial P} \right)_2 - \left(\frac{\partial \phi}{\partial P} \right)_2 \right] \quad , \quad (2.7)$$

$$\frac{\partial}{\partial t} \left(\frac{\phi_5 - \phi_3}{P_5 - P_3} \right) + V_4 \cdot \nabla \left(\frac{\phi_5 - \phi_3}{P_5 - P_3} \right) + \sigma_4 \omega_4 = \frac{1}{\tau} \left[\left(\frac{\partial \phi^*}{\partial P} \right)_4 - \left(\frac{\partial \phi}{\partial P} \right)_4 \right] \quad . \quad (2.8)$$

Equations (2.7) and (2.8) were solved for ω_2 and ω_4 , respectively, and substituted with Equation (2.2) into Equations (2.4), (2.5), and (2.6). These operations yielded the potential vorticity equations

$$\begin{aligned} \frac{\partial}{\partial t} [\nabla^2 \phi_1 + \kappa_2 (\phi_3 - \phi_1)] &= -V_1 \cdot \nabla (\nabla^2 \phi_1 + f_o \beta_o y) - \kappa_2 V_2 \cdot \nabla (\phi_3 - \phi_1) \\ &+ B \nabla^4 \phi_1 + \frac{\kappa_2}{\tau} [\partial \phi_2^* - (\phi_3 - \phi_1)] = C_1, \quad (2.9) \end{aligned}$$

$$\begin{aligned} \frac{\partial}{\partial t} [\nabla^2 \phi_3 + \kappa_4 (\phi_5 - \phi_3) - \kappa_2 (\phi_3 - \phi_1)] &= -V_3 \cdot \nabla (\nabla^2 \phi_3 + f_o \beta_o y) \\ &- \kappa_4 V_4 \cdot \nabla (\phi_5 - \phi_3) + \kappa_2 V_2 \cdot \nabla (\phi_3 - \phi_1) \\ &+ B \nabla^4 \phi_3 + \frac{\kappa_4}{\tau} [\partial \phi_4^* - (\phi_5 - \phi_3)] \\ &- \frac{\kappa_2}{\tau} [\partial \phi_2^* - (\phi_3 - \phi_1)] = C_2, \quad (2.10) \end{aligned}$$

$$\begin{aligned} \frac{\partial}{\partial t} [\nabla^2 \phi_5 - \kappa_6 (\phi_5 - \phi_3)] &= -V_5 \cdot \nabla (\nabla^2 \phi_5 + f_o \beta_o y) + \kappa_6 V_4 \cdot \nabla (\phi_5 - \phi_3) \\ &+ B \nabla^4 \phi_5 - \frac{\kappa_6}{\tau} [\partial \phi_4^* - (\phi_5 - \phi_3)] = C_3, \quad (2.11) \end{aligned}$$

$$\text{where} \quad \kappa_2 = \frac{f_o^2}{\Delta P^2 \sigma_2}, \quad (2.12)$$

$$\kappa_4 = \frac{f_o^2}{\Delta P \pi \sigma_4} = \delta \kappa_2, \quad (2.13)$$

$$\text{and} \quad \kappa_6 = \frac{f_o^2}{P \sigma_6 \pi} = \epsilon \kappa_2. \quad (2.14)$$

A set of three linearly independent eigenvector equations were formed to solve the equation set (2.9), (2.10), and (2.11) after a method by Charney and Phillips (1953). If

$$\Phi = \begin{pmatrix} \phi_1 \\ \phi_3 \\ \phi_5 \end{pmatrix} , \quad (2.15)$$

then the general form of the potential vorticity equation is

$$\nabla^2 \frac{\partial \Phi}{\partial t} + \tilde{A} \kappa_2 \frac{\partial \Phi}{\partial t} = \tilde{C} , \quad (2.16)$$

where

$$\tilde{C} = \begin{pmatrix} C_1 \\ C_2 \\ C_3 \end{pmatrix} ,$$

and \tilde{A} is the appropriate matrix. If

$$\underline{\mu} = \begin{pmatrix} 1 \\ \beta \\ \gamma \end{pmatrix} , \quad (2.17)$$

is an eigenvector of \tilde{A} and λ is its corresponding eigenvalue, then

$$\tilde{A} \underline{\mu} = \lambda \underline{\mu} , \quad (2.18)$$

and

$$A = \begin{pmatrix} -1 & 1 & 0 \\ 1 & -(1+\delta) & \epsilon \\ 0 & \delta & -\epsilon \end{pmatrix} \quad (2.19)$$

Now if

$$\Phi = H_1 u_1 + H_2 u_2 + H_3 u_3 \quad , \quad (2.20)$$

$$\text{and} \quad C = d_1 u_1 + d_2 u_2 + d_3 u_3 \quad , \quad (2.21)$$

are substituted into Equation (2.16) and Equation (2.18) is used to determine the eigenvalues, then the coefficients of each eigenvector can be equated to give

$$\frac{\partial}{\partial t} [(\nabla^2 + \lambda_i \kappa_2) H_i] = d_i \quad , \quad (2.22)$$

where $i = 1, 2, 3$.

The following eigenvalues as specified by Equation (2.18) were obtained,

$$\left. \begin{aligned} \lambda_1 &= 0 \\ \lambda_2 &= -\frac{1}{2} (2+\delta+\epsilon) + \frac{1}{2} [(\epsilon+\delta)^2 + 4(1-\epsilon)]^{\frac{1}{2}} \\ \lambda_3 &= -\frac{1}{2} (2+\delta+\epsilon) - \frac{1}{2} [(\epsilon+\delta)^2 + 4(1-\epsilon)]^{\frac{1}{2}} \end{aligned} \right\} \quad (2.23)$$

The eigenvector equation set was formed from the potential vorticity equations (2.9), (2.10), and (2.11) and Equation (2.22). These equations are

$$\begin{aligned} \frac{\partial}{\partial t} [\nabla^2 H_1] = & -\nabla \cdot [\beta_0 y k x \nabla H_1 + V_1 \nabla^2 \phi_1 + V_3 \nabla^2 \phi_3 + V_5 \nabla^2 \frac{\delta}{\epsilon} \phi_5] \\ & + B \nabla^2 H_1 + Q \quad , \end{aligned} \quad (2.24)$$

$$\begin{aligned} \frac{\partial}{\partial t} [(\nabla^2 + \lambda_2 \kappa_2) H_2] = & -\nabla \cdot \{ \beta_0 y k x \nabla H_2 + V_1 \nabla^2 \phi_1 + \beta_2 V_3 \nabla^2 \phi_3 + \gamma_2 V_5 \nabla^2 \phi_5 \\ & - \lambda_2 \kappa_2 [V_2 (\phi_3 - \phi_1) - \gamma_2 V_4 (\phi_5 - \phi_3)] \} + B \nabla^4 H_2 + Q \quad , \end{aligned} \quad (2.25)$$

$$\begin{aligned} \frac{\partial}{\partial t} [(\nabla^2 + \lambda_3 \kappa_2) H_3] = & -\nabla \cdot \{ \beta_0 y k x \nabla H_3 + V_1 \nabla^2 \phi_1 + \beta_3 V_3 \nabla^2 \phi_3 + \gamma_3 V_5 \nabla^2 \phi_5 \\ & - \lambda_3 \kappa_2 [V_2 (\phi_3 - \phi_1) - \gamma_3 V_4 (\phi_5 - \phi_3)] \} + B \nabla^4 H_3 + Q \quad , \end{aligned} \quad (2.26)$$

$$\text{where } Q = \frac{\kappa_2}{\tau} [(1-\beta)(\partial \phi_2^* - \partial \phi_2) + (\partial \beta - \gamma \epsilon)(\partial \phi_4^* - \partial \phi_4)] \quad . \quad (2.27)$$

An assumed solution of the form

$$H = \bar{H}(y, t) + H_c \cos kx + H_s \sin kx \quad , \quad (2.28)$$

where \bar{H} is the zonal mean solution amplitude, H_c is the Fourier cosine eddy amplitude, and H_s is the Fourier sine eddy amplitude, was introduced into Equations (2.24), (2.25), and (2.26) as suggested by Lorenz (1960). The equations were quasi-linearized by eliminating all terms of higher

wave number than k . This technique permits full interaction of the disturbance in x with the mean flow, but neglects interaction with the other waves in x .

Equations (2.24), (2.25), and (2.26) were separated into components independent of x , coefficients of $\cos kx$, and coefficients of $\sin kx$. The resulting equation set (2.29) through (2.43) constitute the prediction equations for this model. The primed quantities represent the partial derivative with respect to y .

The terms independent of x in (2.24) give:

$$\begin{aligned} \frac{\partial}{\partial t} H'' = & -\frac{k}{2f_0} [(\phi_{1c}''' \phi_{1s} - \phi_{1s}''' \phi_{1c}) - (\phi_{1s}'' \phi_{1c}' - \phi_{1c}'' \phi_{1s}') \\ & + (\phi_{3c}''' \phi_{3s} - \phi_{3s}''' \phi_{3c}) - (\phi_{3s}'' \phi_{3c}' - \phi_{3c}'' \phi_{3s}') \\ & + \frac{\delta}{\epsilon} (\phi_{5c}''' \phi_{5s} - \phi_{5s}''' \phi_{5c}) - \frac{\delta}{\epsilon} (\phi_{5s}'' \phi_{5c}' - \phi_{5c}'' \phi_{5s}')] \\ & + \bar{F} + \bar{Q} \quad , \end{aligned} \quad (2.29)$$

$$\text{where} \quad \bar{F} = B \bar{H}'''' \quad , \quad (2.30)$$

$$\text{and} \quad \bar{Q} = \frac{\kappa_2}{\tau} [(1-\beta)(\partial \phi_2^* - \partial \bar{\phi}_2) + (\delta\beta - \gamma\epsilon)(\partial \phi_4^* - \partial \bar{\phi}_4)] \quad . \quad (2.31)$$

The $\cos kx$ terms in (2.24) give:

$$\begin{aligned}
 \frac{\partial}{\partial t} \left(\frac{\partial^2}{\partial y^2} - k^2 \right) H_c = & - \frac{k}{f_o} [\beta_o H_s f_o + (\bar{\phi}_1''' + k^2 \bar{\phi}_1' \phi_{1s} - \bar{\phi}_1' \phi_{1s}'') \\
 & + (\bar{\phi}_3''' + k^2 \bar{\phi}_3' \phi_{3s} - \bar{\phi}_3' \phi_{3s}'') \\
 & + \frac{\delta}{\epsilon} (\bar{\phi}_5''' + k^2 \bar{\phi}_5' \phi_{5s} - \bar{\phi}_5' \phi_{5s}'')] + F_c + Q_c,
 \end{aligned} \tag{2.32}$$

$$\text{where } F_c = B(H_c'''' - 2k^2 H_c'' + k^4 H_c) \quad , \tag{2.33}$$

$$\text{and } Q_c = \frac{\kappa_2}{\tau} [(1-\beta)(\partial \phi_2^* - \partial \phi_{2c}) + (\delta\beta - \gamma\epsilon)(\partial \phi_4^* - \partial \phi_{4c})] \quad . \tag{2.34}$$

The $\sin kx$ terms in (2.24) give:

$$\begin{aligned}
 \frac{\partial}{\partial t} \left(\frac{\partial^2}{\partial y^2} - k^2 \right) H_s = & - \frac{k}{f_o} [\beta_o f_o H_c + (\bar{\phi}_1''' \phi_{1c} + k^2 \bar{\phi}_1' \phi_{1c} - \bar{\phi}_1' \phi_{1c}'') \\
 & + (\bar{\phi}_3''' \phi_{3c} + k^2 \bar{\phi}_3' \phi_{3c} - \bar{\phi}_3' \phi_{3c}'') \\
 & + \frac{\delta}{\epsilon} (\bar{\phi}_5''' \phi_{5c} + k^2 \bar{\phi}_5' \phi_{5c} - \bar{\phi}_5' \phi_{5c}'')] + F_s + Q_s,
 \end{aligned} \tag{2.35}$$

$$\text{where } F_s = B(H_s'''' - 2k^2 H_s'' + k^4 H_s) \quad , \tag{2.36}$$

$$\text{and } Q_s = \frac{\kappa_2}{\tau} [(1-\beta)(\partial \phi_2^* - \partial \phi_{2s}) + (\delta\beta - \gamma\epsilon)(\partial \phi_4^* - \partial \phi_{4s})] \quad . \tag{2.37}$$

The terms independent of x in (2.25) give:

$$\begin{aligned}
\frac{\partial}{\partial t} \left(\frac{\partial^2}{\partial y^2} + \lambda_2 \kappa_2 \right) \bar{H} = & - \frac{k}{2f_0} \{ (\phi_{1c}''' \phi_{1s} - \phi_{1s}''' \phi_{1c}) - (\phi_{1s}'' \phi_{1c}' - \phi_{1c}'' \phi_{1s}') \\
& + \beta_2 [(\phi_{3c}''' \phi_{3s} - \phi_{3s}''' \phi_{3c}) - (\phi_{3s}'' \phi_{3c}' - \phi_{3c}'' \phi_{3s}')] \\
& + \gamma_2 [(\phi_{5c}''' \phi_{5s} - \phi_{5s}''' \phi_{5c}) - (\phi_{5s}'' \phi_{5c}' - \phi_{5c}'' \phi_{5s}')] \\
& - \lambda_2 \kappa_2 [(\phi_{3c}' \phi_{1s} - \phi_{3s}' \phi_{1c}) - (\phi_{1c}' \phi_{3s} - \phi_{1s}' \phi_{3c}) \\
& - \gamma_2 (\phi_{5c}' \phi_{3s} - \phi_{5s}' \phi_{3c}) + \gamma_2 (\phi_{3c}' \phi_{5s} - \phi_{3s}' \phi_{5c})] \} \\
& + \bar{F} + \bar{Q} \quad , \quad (2.38)
\end{aligned}$$

The $\cos kx$ terms in (2.25) give:

$$\begin{aligned}
\frac{\partial}{\partial t} \left(\frac{\partial^2}{\partial y^2} - k^2 + \lambda_2 \kappa_2 \right) H_c = & - \frac{k}{f_0} \{ \beta_0 f_0 H_s + (\bar{\phi}_1''' \phi_{1s} + k^2 \bar{\phi}_1' \phi_{1s} - \bar{\phi}_1' \phi_{1s}'') \\
& + \beta_2 (\bar{\phi}_3''' \phi_{3s} + k^2 \bar{\phi}_3' \phi_{3s} - \bar{\phi}_3' \phi_{3s}'') \\
& + \gamma_2 (\bar{\phi}_5''' \phi_{5s} + k^2 \bar{\phi}_5' \phi_{5s} - \bar{\phi}_5' \phi_{5s}'') \\
& + \lambda_2 \kappa_2 [(\bar{\phi}_1' \phi_{3s} - \bar{\phi}_3' \phi_{1s}) + \gamma_2 (\bar{\phi}_5' \phi_{3s} - \bar{\phi}_3' \phi_{5s})] \} + F_c + Q_c, \quad (2.39)
\end{aligned}$$

The $\sin kx$ terms in (2.25) give:

$$\begin{aligned}
\frac{\partial}{\partial t} \left(\frac{\partial^2}{\partial y^2} - k^2 + \lambda_2 \kappa_2 \right) H_s = & - \frac{k}{f_0} \{ \beta_0 f_0 H_c + (\bar{\phi}_1''' \phi_{1c} + k^2 \bar{\phi}_1' \phi_{1c} - \bar{\phi}_1' \phi_{1c}'') \\
& + \beta_2 (\bar{\phi}_3''' \phi_{3c} + k^2 \bar{\phi}_3' \phi_{3c} - \bar{\phi}_3' \phi_{3c}'') \\
& + \gamma_2 (\bar{\phi}_5''' \phi_{5c} + k^2 \bar{\phi}_5' \phi_{5c} - \bar{\phi}_5' \phi_{5c}'') \\
& + \lambda_2 \kappa_2 [(\bar{\phi}_1' \phi_{3c} - \bar{\phi}_3' \phi_{1c}) + \gamma_2 (\bar{\phi}_5' \phi_{3c} - \bar{\phi}_3' \phi_{5c})] \} + F_s + Q_s,
\end{aligned} \tag{2.40}$$

The terms independent of x in (2.26) give:

$$\begin{aligned}
\frac{\partial}{\partial t} \left(\frac{\partial^2}{\partial y^2} + \lambda_3 \kappa_2 \right) \bar{H} = & - \frac{k}{2f_0} \{ (\phi_{1c}''' \phi_{1s} - \phi_{1s}''' \phi_{1c}) - (\phi_{1s}'' \phi_{1c}' - \phi_{1c}'' \phi_{1s}') \\
& + \beta_3 [(\phi_{3c}''' \phi_{3s} - \phi_{3s}''' \phi_{3c}) - (\phi_{3s}'' \phi_{3c}' - \phi_{3c}'' \phi_{3s}')] \\
& + \gamma_3 [(\phi_{5c}''' \phi_{5s} - \phi_{5s}''' \phi_{5c}) - (\phi_{5s}'' \phi_{5c}' - \phi_{5c}'' \phi_{5s}')] \\
& - \lambda_3 \kappa_2 [(\phi_{3c}' \phi_{1s} - \phi_{3s}' \phi_{1c}) - (\phi_{1c}' \phi_{3s} - \phi_{1s}' \phi_{3c}) \\
& - \gamma_3 (\phi_{5c}' \phi_{3s} - \phi_{5s}' \phi_{3c}) + \gamma_3 (\phi_{3c}' \phi_{5s} - \phi_{3s}' \phi_{5c})] \} \\
& + \bar{F} + \bar{Q},
\end{aligned} \tag{2.41}$$

The $\cos kx$ terms in (2.26) give:

$$\begin{aligned} \frac{\partial}{\partial t} \left(\frac{\partial^2}{\partial y^2} - k^2 + \lambda_3 \kappa_2 \right) H_c = & - \frac{k}{f_0} \{ \beta_0 f_0 H_s + (\bar{\phi}_1''' \phi_{1s} + k^2 \bar{\phi}_1' \phi_{1s} - \bar{\phi}_1' \phi_{1s}'') \\ & + \beta_3 (\bar{\phi}_3''' + k^2 \bar{\phi}_3' \phi_{3s} - \bar{\phi}_3' \phi_{3s}'') + \gamma_3 (\bar{\phi}_5''' \phi_{5s} + k^2 \bar{\phi}_5' \phi_{5s} - \bar{\phi}_5' \phi_{5s}'') \\ & + \lambda_3 \kappa_2 [(\bar{\phi}_1' \phi_{3s} - \bar{\phi}_3' \phi_{1s}) + \gamma_3 (\bar{\phi}_5' \phi_{3s} - \bar{\phi}_3' \phi_{5s})] \} + F_c + Q_c, \end{aligned} \quad (2.42)$$

The $\sin kx$ terms in (2.26) give:

$$\begin{aligned} \frac{\partial}{\partial t} \left(\frac{\partial^2}{\partial y^2} - k^2 + \lambda_3 \kappa_2 \right) H_s = & - \frac{k}{f_0} \{ \beta_0 f_0 H_c + (\bar{\phi}_1''' \phi_{1c} + k^2 \bar{\phi}_1' \phi_{1c} - \bar{\phi}_1' \phi_{1c}'') \\ & + \beta_3 (\bar{\phi}_3''' \phi_{3c} + k^2 \bar{\phi}_3' \phi_{3c} - \bar{\phi}_3' \phi_{3c}'') \\ & + \gamma_3 (\bar{\phi}_5''' \phi_{5c} + k^2 \bar{\phi}_5' \phi_{5c} - \bar{\phi}_5' \phi_{5c}'') \\ & + \lambda_3 \kappa_2 [(\bar{\phi}_1' \phi_{3c} - \bar{\phi}_3' \phi_{1c}) + \gamma_3 (\bar{\phi}_5' \phi_{3c} - \bar{\phi}_3' \phi_{5c})] \} + F_s + Q_s. \end{aligned} \quad (2.43)$$

A method developed by Richtmeyer (1957) was used to solve for the tendency, $\frac{\partial H}{\partial t}$, at each time step. The equations were integrated in time by a marching process. All finite differences were centered in time or space. A forward time step was used to start the marching process. A finite difference scheme developed by Matsuno (1966) was

used every 50 time steps. This is a two step iteration to simulate the backward difference method. This scheme was applied in this situation to suppress the computational mode that would arise from using the centered time differencing exclusively. A time step of 30 minutes was used.

III. RESULTS

Two experiments were conducted under varied conditions. The first experiment was designed to yield the growth rate of the most unstable wave in the disturbance fields for Rossby deformation lengths of 75 KM and 750 KM. This range of values for the Rossby deformation length was suggested by Gierasch (1973). The upper two levels each had a pressure differential of 50 CB, while thickness of the lowest level assumed values of 50, 500, and 5000 CB, respectively. The y-wavelength of the mean flow was 15,000 KM for all cases. The x-wavelength varied from 1,000 KM to 15,000 KM for $R_L = 750$ KM and from 300 KM to 3000 KM for $R_L = 75$ KM. κ_2 as defined by Equation (2.12) was scaled to be

$$\kappa_2 = \frac{1}{R_L^2} . \quad (3.1)$$

The static stability at level 2, σ_2 , was obtained from Equation (3.1) and the static stability at level 4, σ_4 , was found by the relation

$$\sigma_4 = \sigma_2 \frac{P_2^2}{P_4^2} , \quad (3.2)$$

where P_2 and P_4 are the absolute pressures at levels 2 and 4, respectively. This ratio was a constant equal to 0.25 for all experiments. The mean wind U_0 was initialized as

a sinusoidal function of y with an amplitude of 20.5 meters per second in level 1. This value was obtained from $U_0 = \beta/k_y^2$ which is the limiting value for barotropic stability as suggested by Ingersoll and Cuzzi (1969). The mean wind was zero in levels 3 and 5. The mean field was held constant, which makes the equations linear, throughout the first experiment. The disturbance field $\cos kx$ contained an initial sinusoidal variation with the same y -scale as the mean flow and an amplitude an order of magnitude smaller than the mean field. The initial $\sin kx$ field was entirely described by the $\cos kx$ terms. There were no heating or friction terms included.

The forecasts were carried forward until the growth rates became exponential. Growth rates of the disturbance were calculated by

$$\frac{1}{A} \frac{\partial A}{\partial t} = M = \frac{1}{t_2 - t_1} \ln \frac{A_2}{A_1}, \quad (3.3)$$

where M is the exponential growth rate, A is the amplitude of the disturbance, and t_2 and t_1 are the times at which the disturbance amplitudes were A_2 and A_1 , respectively. The maximum growth rate for $R_L = 750$ KM occurred at an x -wavelength of 6,000 KM for all lower layer thicknesses (Figure 2). For lower layer thicknesses of 50 and 500 CB and $R_L = 75$ KM the maximum growth rate was at an x -wavelength of 600 KM. The 5000 CB case showed maximum growth rate at an x -wavelength of 500 KM (Figure 3).

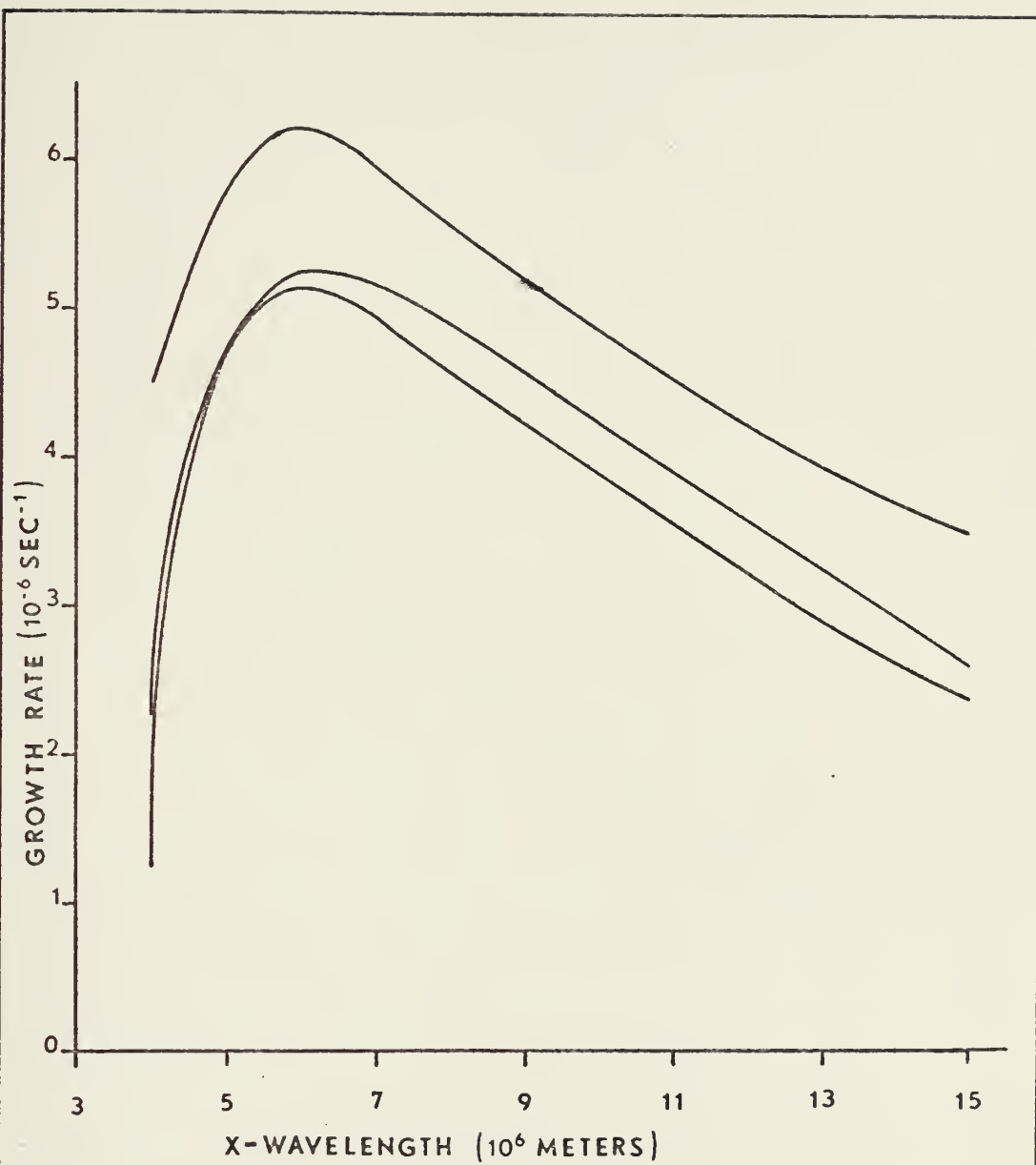


FIGURE 2 - Growth Rate of Y-Disturbance Wave for $R_L = 750$ KM

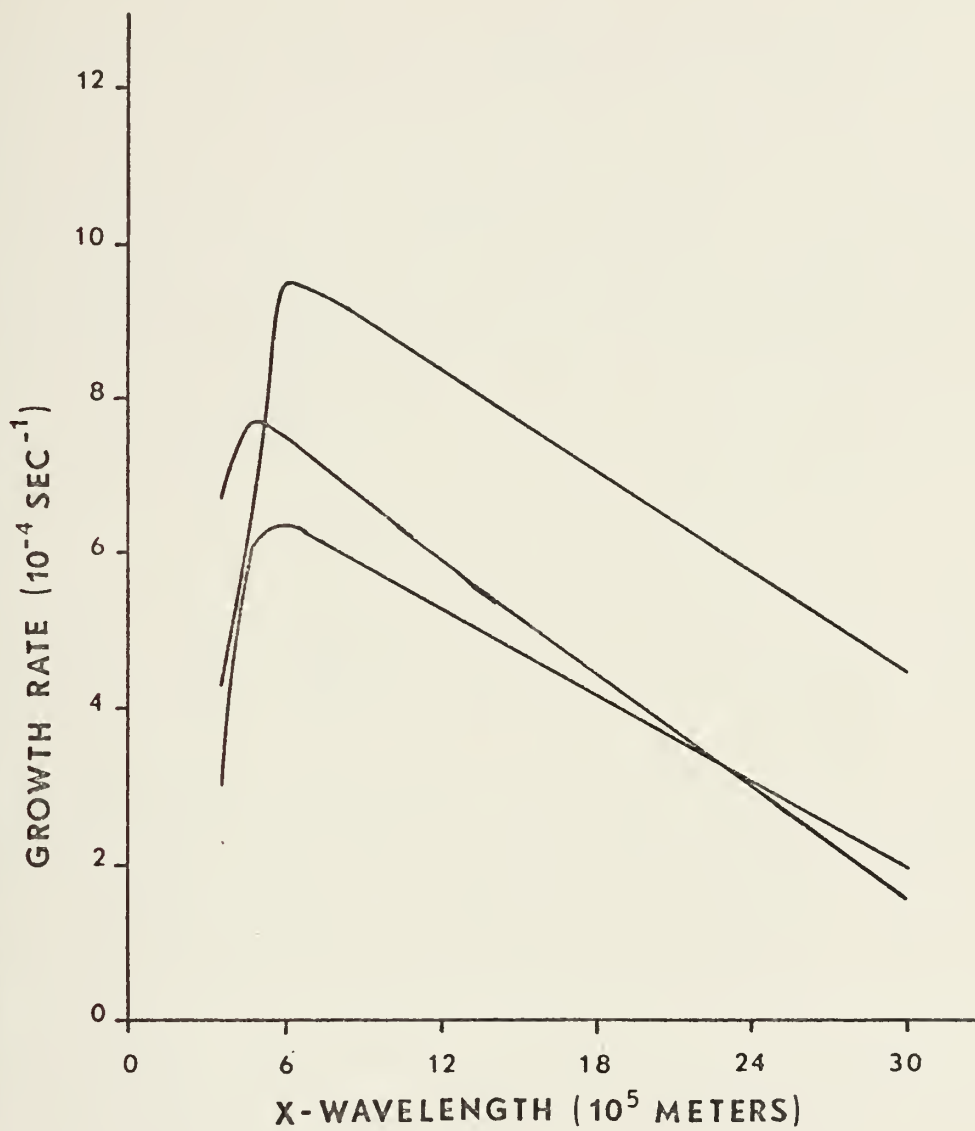


FIGURE 3 - Growth Rate of Y-Disturbance Wave for $R_L = 75$ KM

The phase and amplitude relationships of the disturbance field were determined by

$$\phi_c \cos kx + \phi_s \sin kx = C \cos(kx - \delta), \quad (3.4)$$

where ϕ_c and ϕ_s are the geopotentials in the $\cos kx$ and $\sin kx$ fields, respectively. Equation (3.4) was expanded to yield the following expressions for the amplitude C and the phase angle δ ,

$$\delta = \arctan \left(\frac{\phi_s}{\phi_c} \right), \quad (3.5)$$

$$C = \frac{\phi_c}{\cos \delta} = \frac{\phi_s}{\sin \delta}. \quad (3.6)$$

The amplitude and phase relationships for ϕ_1 , ϕ_3 , and ϕ_5 were computed at the maximum growth rate for each case. The results are shown in Figures 4 through 15. All amplitude profiles showed greater relative growth in the northern wave; however, the effect was more pronounced at $R_L = 750$ KM. This was due to the presence of the planetary vorticity gradient β . The relative amplitudes of ϕ_1 , ϕ_3 , and ϕ_5 were the same order of magnitude for the lower level thickness $P = 50$ CB (Figures 4 and 7). The amplitude of ϕ_5 was an order of magnitude smaller than ϕ_1 or ϕ_3 for $P = 500$ CB (Figures 5 and 8). At $P = 5000$ CB (Figures 6 and 9) the amplitude of ϕ_5 was negligible compared to ϕ_1 or ϕ_3 . These characteristics were observed at both values

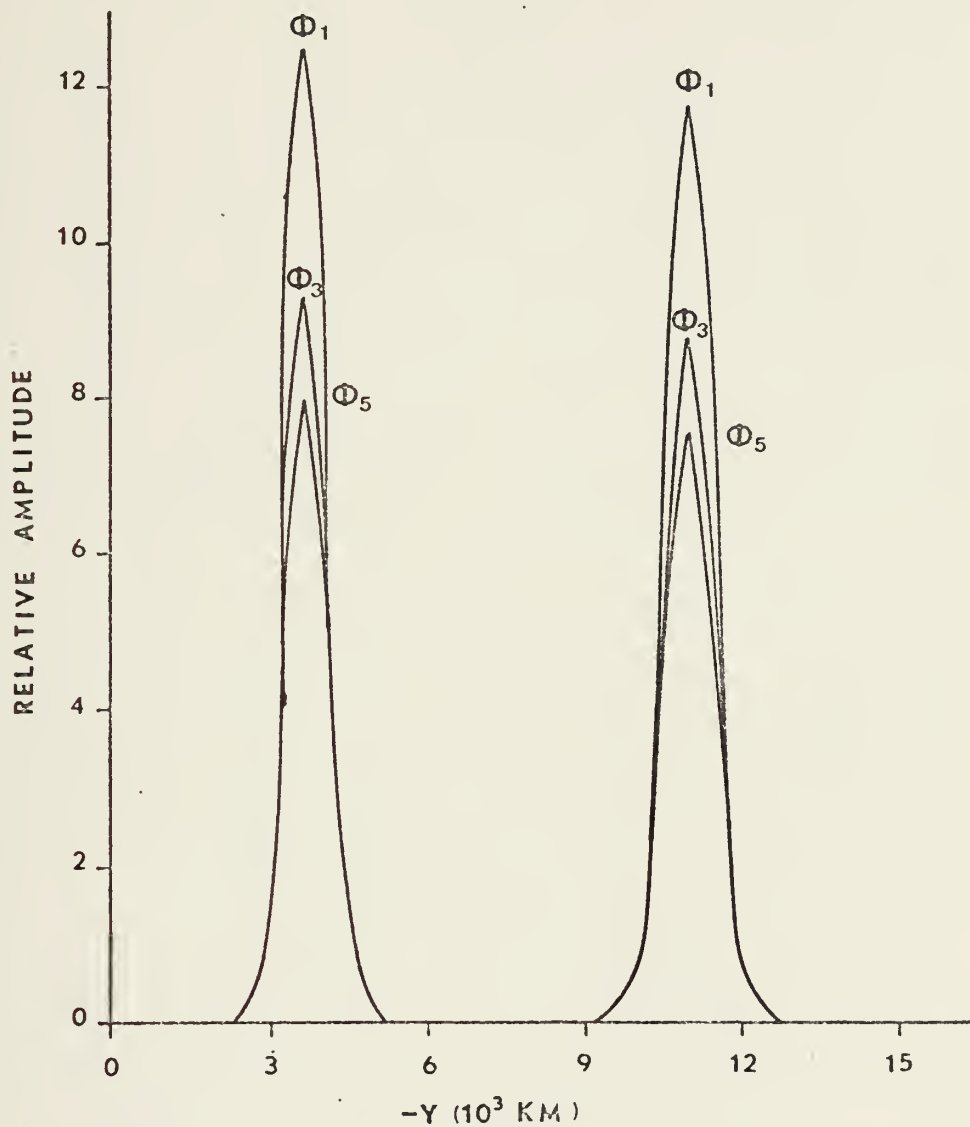


FIGURE 4 - Relative Amplitude of ϕ_1 , ϕ_3 , and ϕ_5 as a Function of Y for $\Delta P=50$ CB, $R_L = 75$ KM, and x-wavelength of 600 KM. Y-Axis has been shifted to the north.

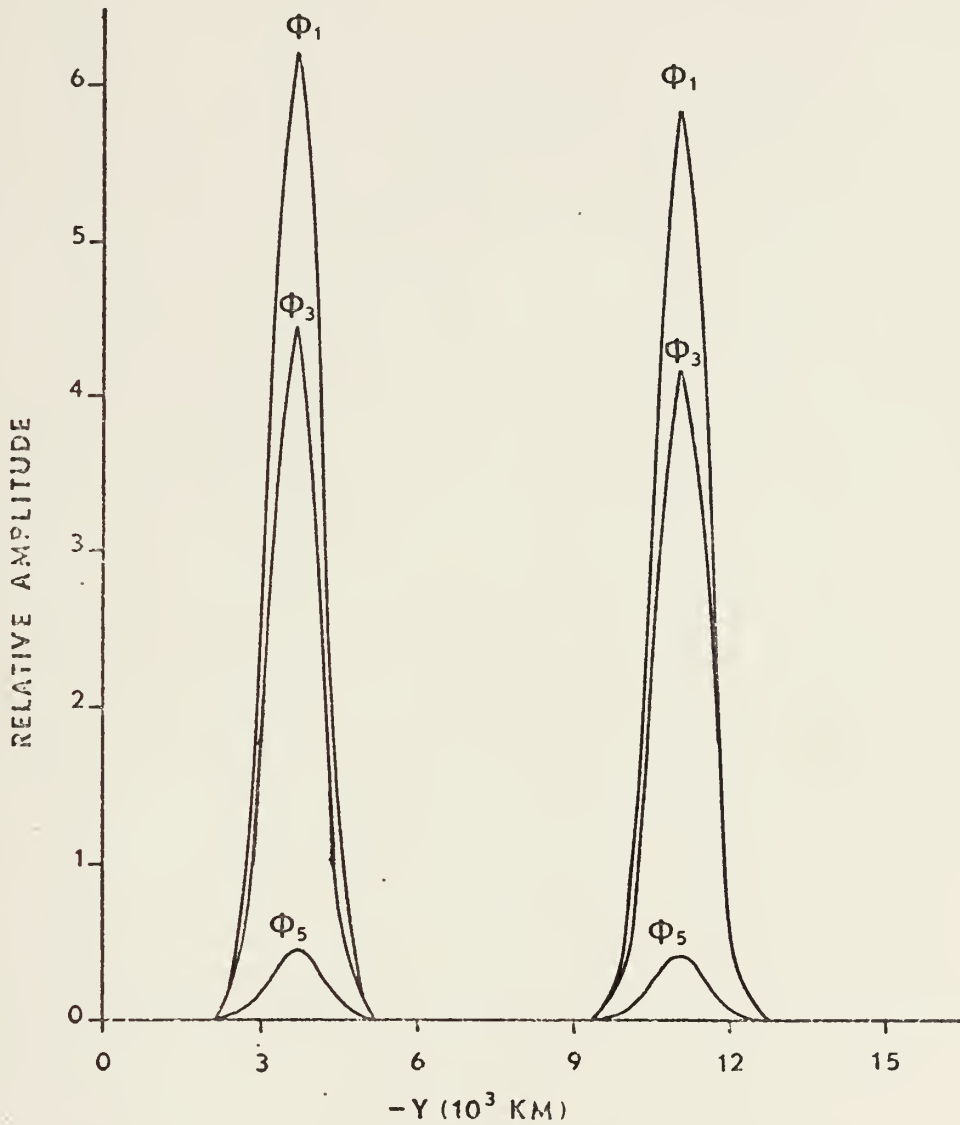


FIGURE 5 - Relative Amplitude of ϕ_1 , ϕ_3 , and ϕ_5 as a Function of Y for $\Delta P = 50$ CB, $P = 500$ CB, $R_L = 75$ KM, and x -wavelength of 600 KM.

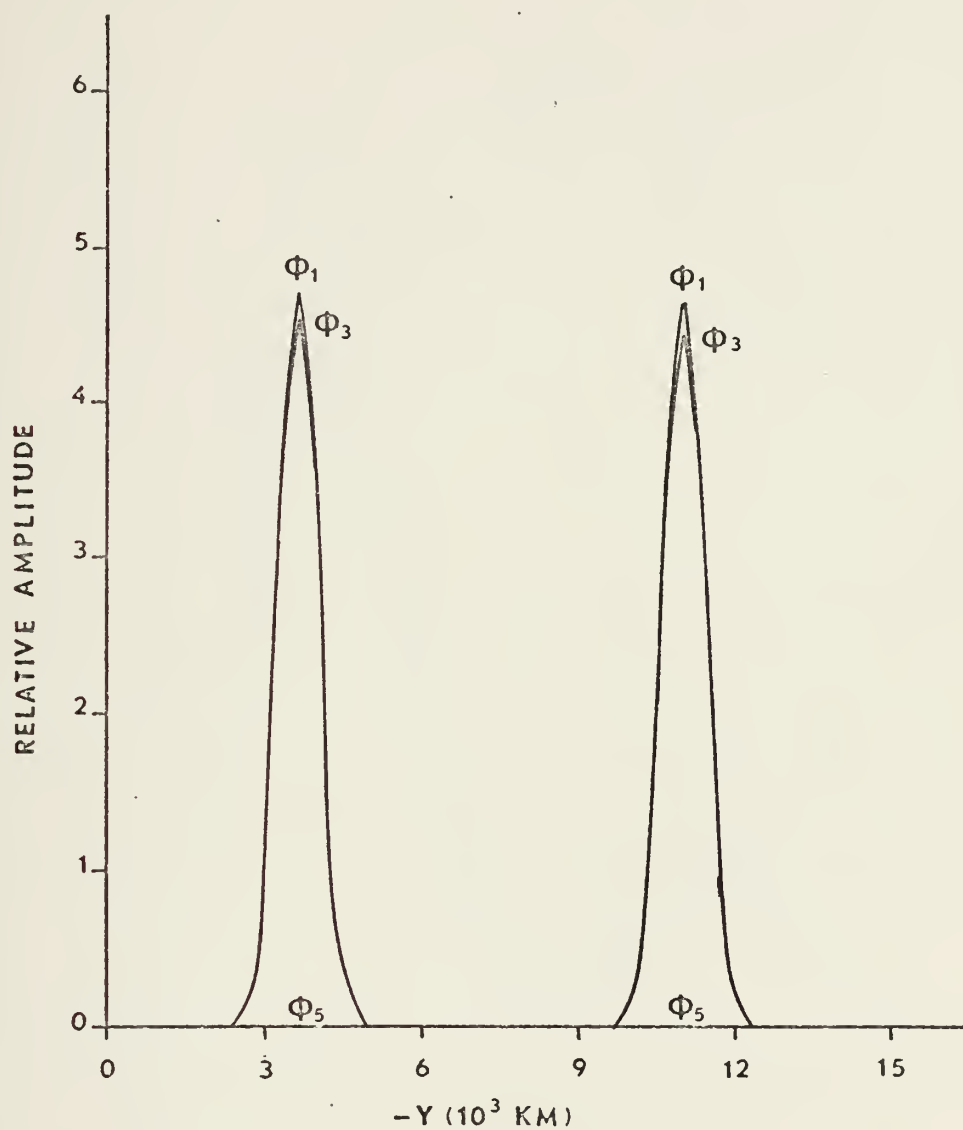


FIGURE 6 - Relative Amplitude of ϕ_1 , ϕ_3 , and ϕ_5 as a Function of Y for $\Delta P = 50$ CB, $P = 5000$ CB, $R_L = 75$ KM, and x -wavelength of 600 KM.

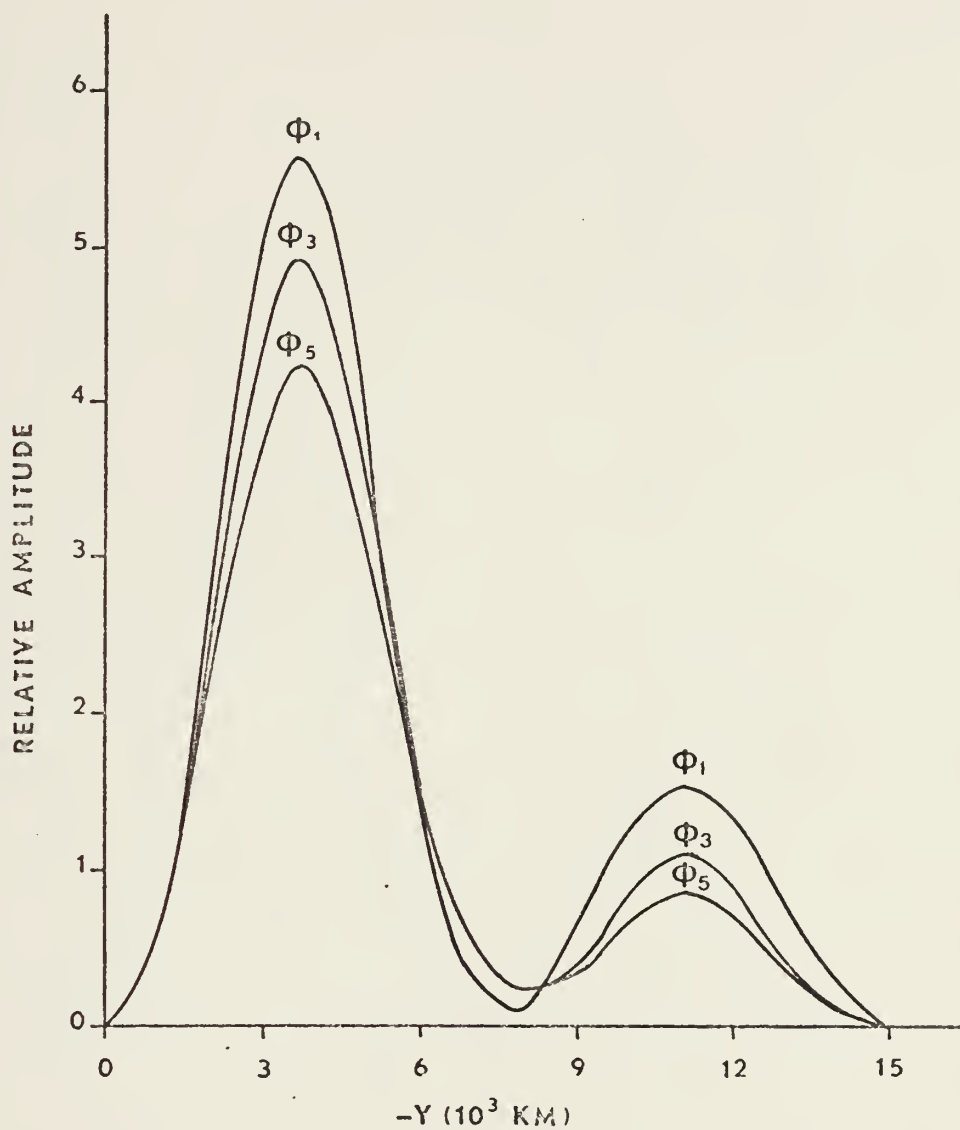


FIGURE 7 - Relative Amplitude of ϕ_1 , ϕ_3 , and ϕ_5 as a Function of Y for $\Delta P = 50$ CB, $P = 50$ CB, $R_L = 750$ KM, and x -wavelength of 6000 KM.

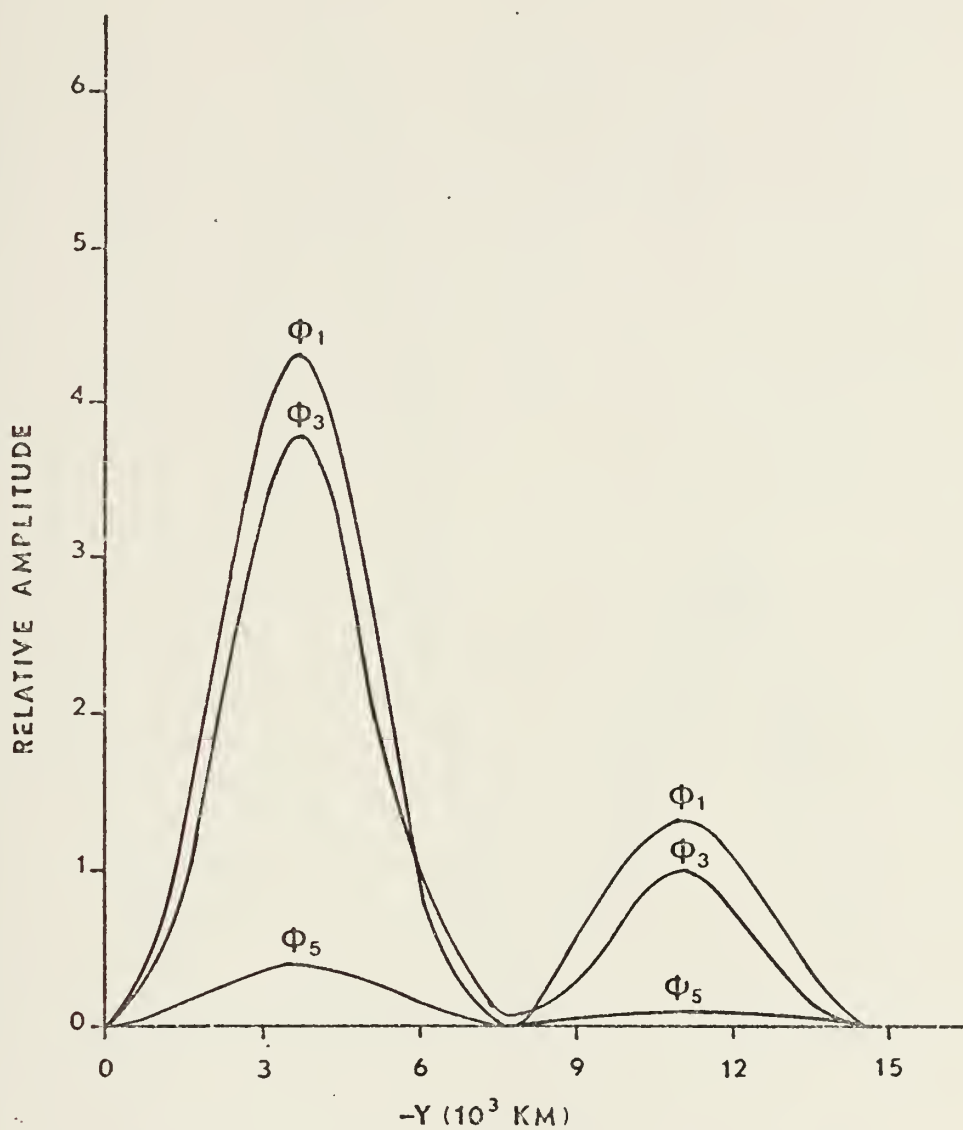


FIGURE 8 - Relative Amplitude of ϕ_1 , ϕ_3 , and ϕ_5 as a Function of Y for $\Delta P = 50$ CB, $P = 500$ CB, $R_L = 750$ KM, and x -wavelength of 6000 KM.



FIGURE 9 - Relative Amplitude of ϕ_1 , ϕ_3 , and ϕ_5 as a Function of Y for $\Delta P = 50$ CB, $P = 5000$ CB, $R_L = 750$ KM, and x -wavelength of 6000 KM.

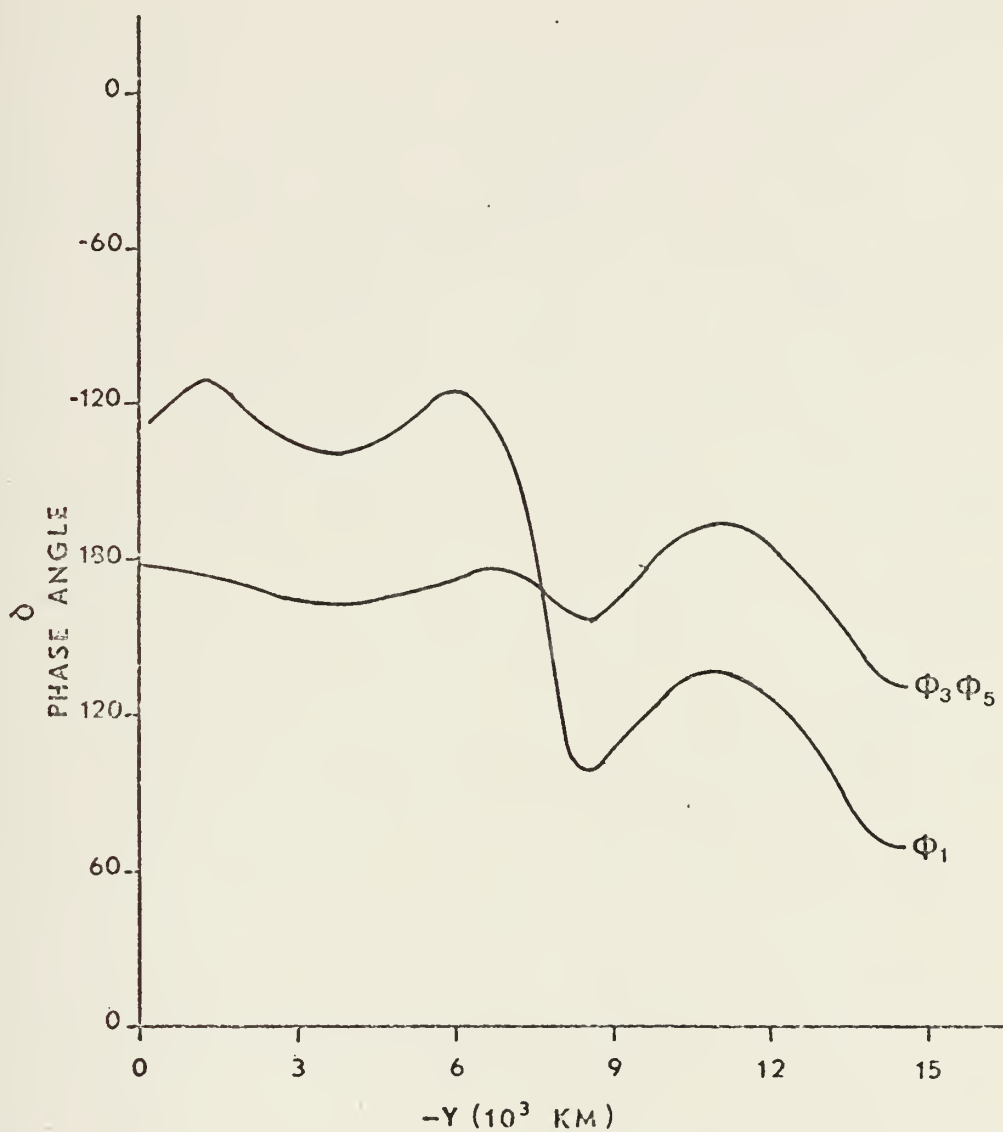


FIGURE 10 - Phase Angles of ϕ_1 , ϕ_3 , and ϕ_5 as a Function of Y for $\Delta P = 50$ CB, $P = 50$ CB, $R_L = 750$ KM, and x -wavelength of 6000 KM.

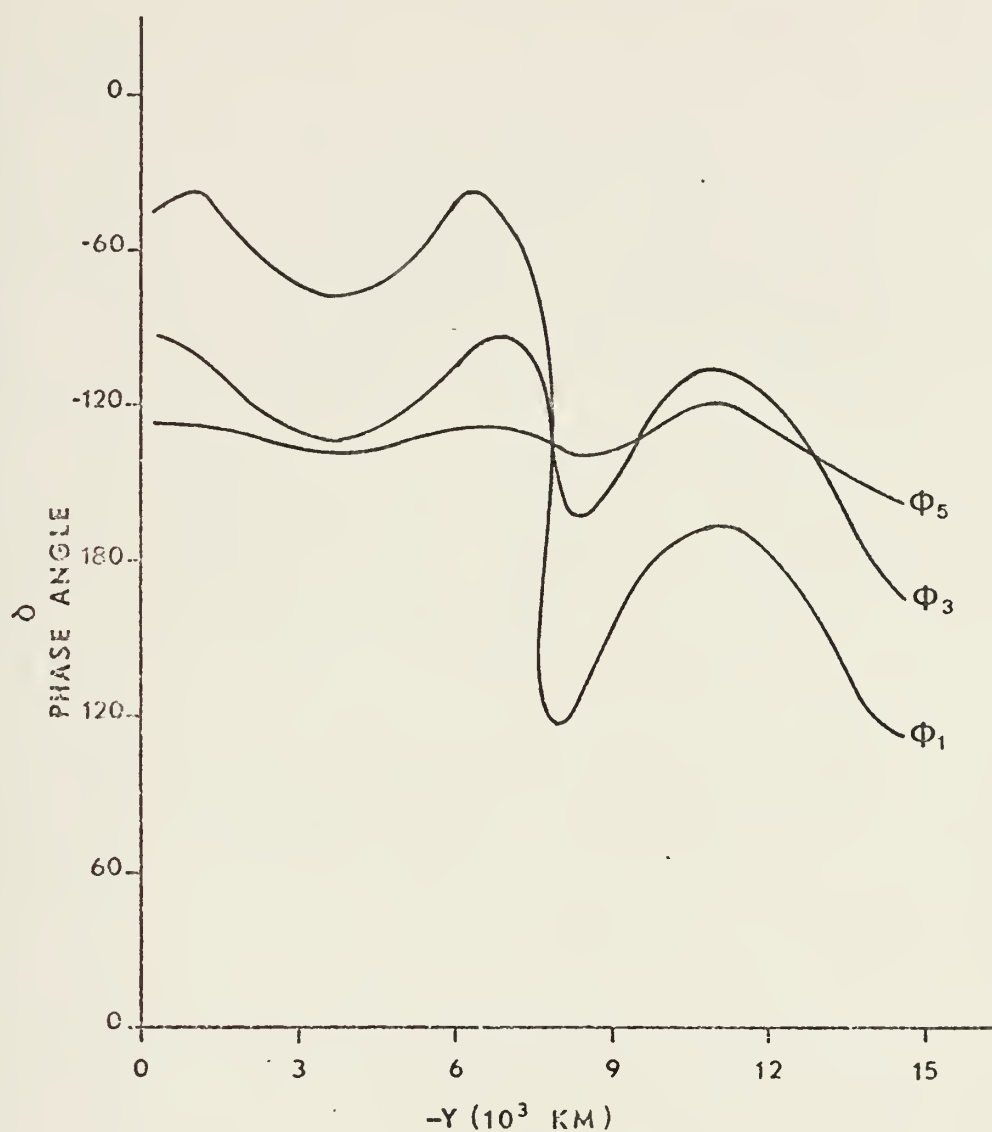


FIGURE 11 - Phase Angles of ϕ_1 , ϕ_3 , and ϕ_5 as a Function of Y for $\Delta P = 50$ CB, $P = 500$ CB, $R_L = 750$ KM, and x -wavelength of 6000 KM.

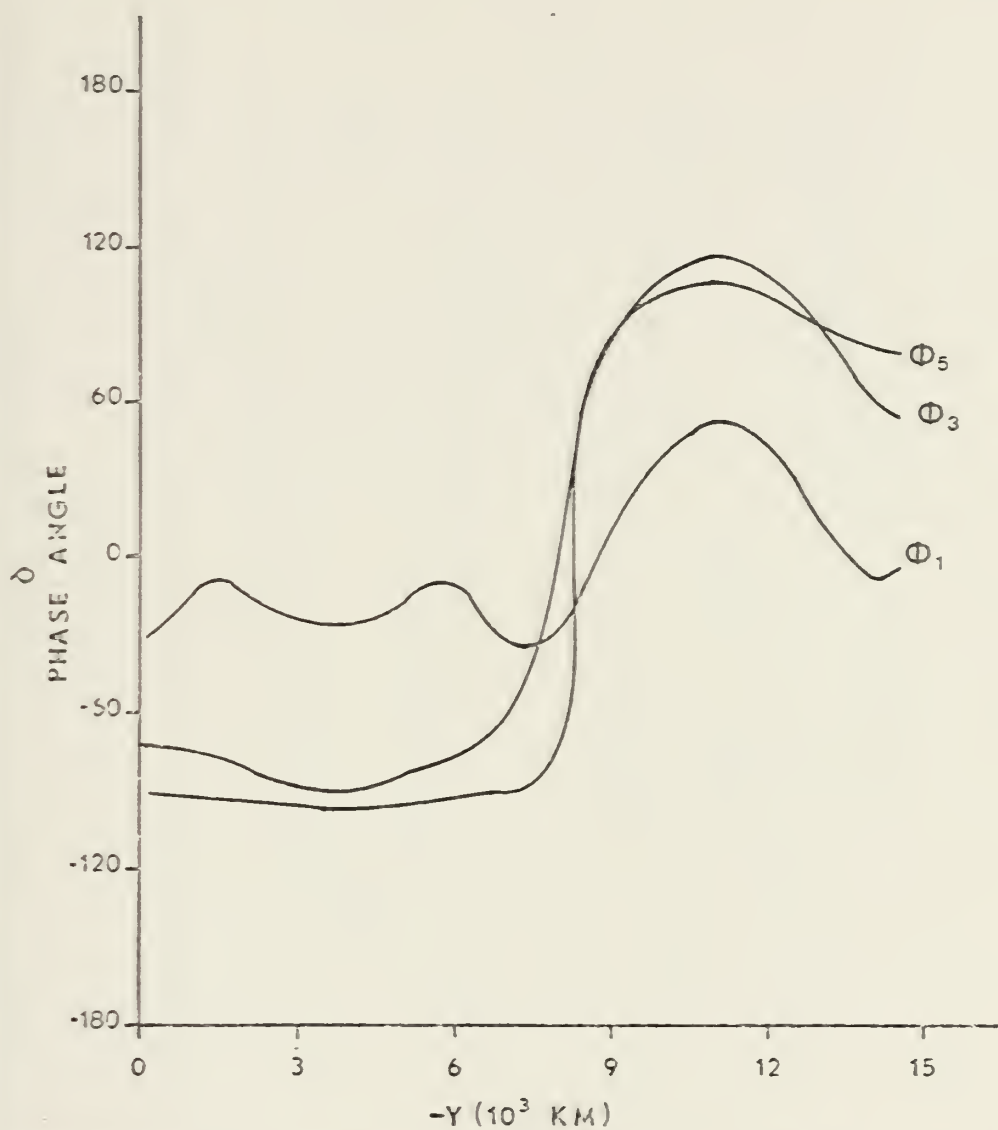


FIGURE 12 - Phase Angles of ϕ_1 , ϕ_3 , and ϕ_5 as a Function of Y for $\Delta P = 50$ CB, $P = 5000$ CB, $R_L = 750$ KM, and x -wavelength of 6000 KM.

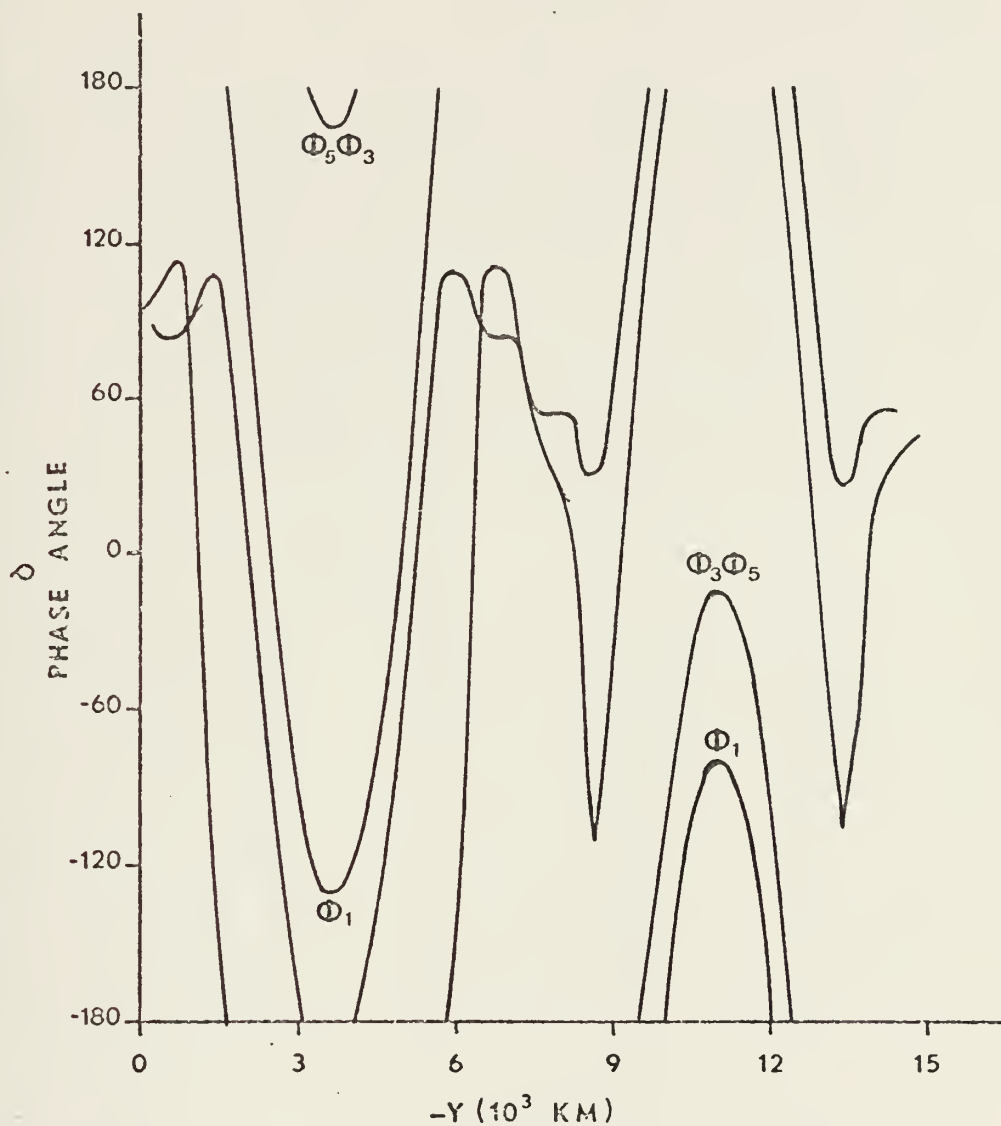


FIGURE 13 - Phase Angles of ϕ_1 , ϕ_3 , and ϕ_5 as a Function of Y for $\Delta P = 50$ CB, $P = 50$ CB, $R_L = 75$ KM, and x -wavelength of 600 KM.

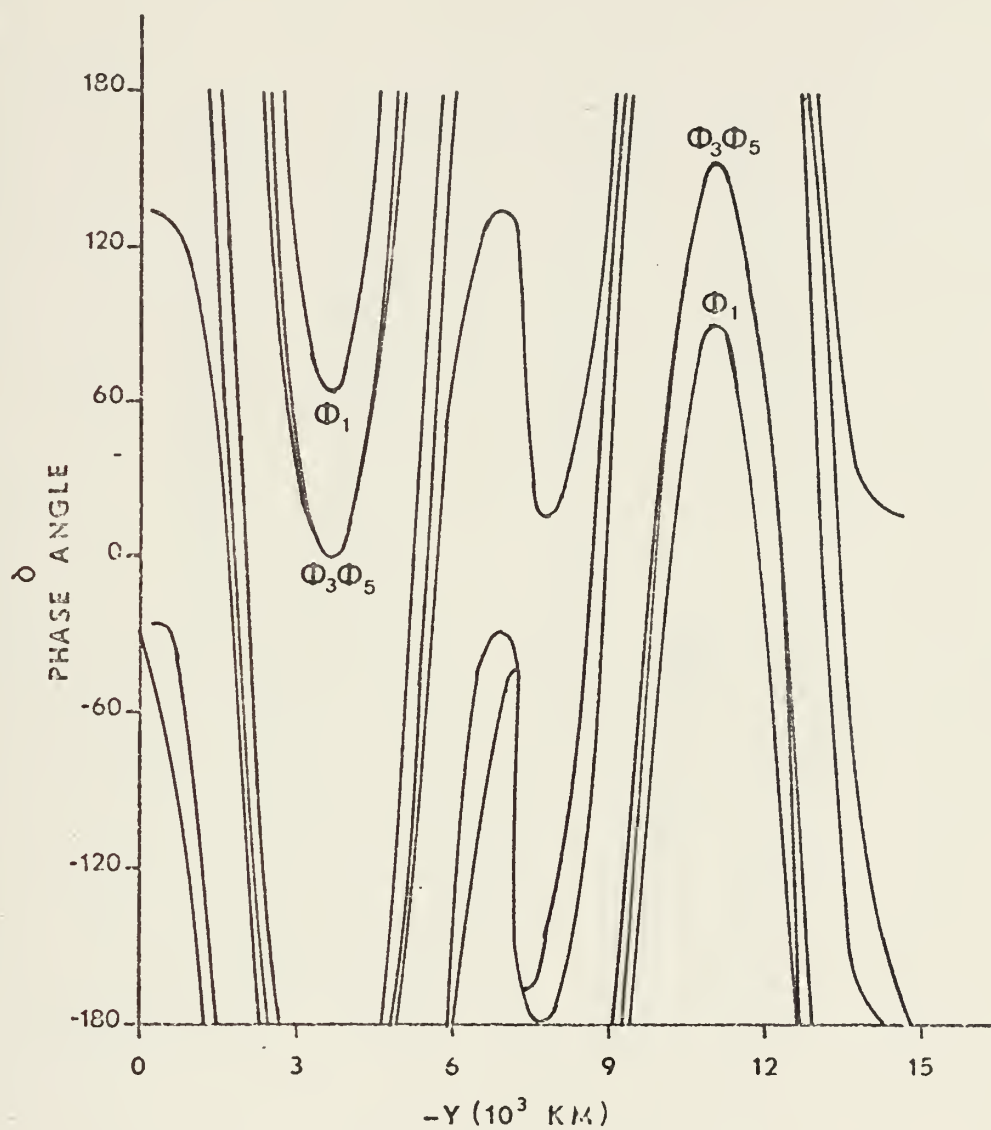


FIGURE 14 - Phase Angles of ϕ_1 , ϕ_3 , and ϕ_5 as a Function of Y for $\Delta P = 50$ CB, $P = 500$ CB, $R_L = 75$ KM, and x-wavelength of 600 KM.

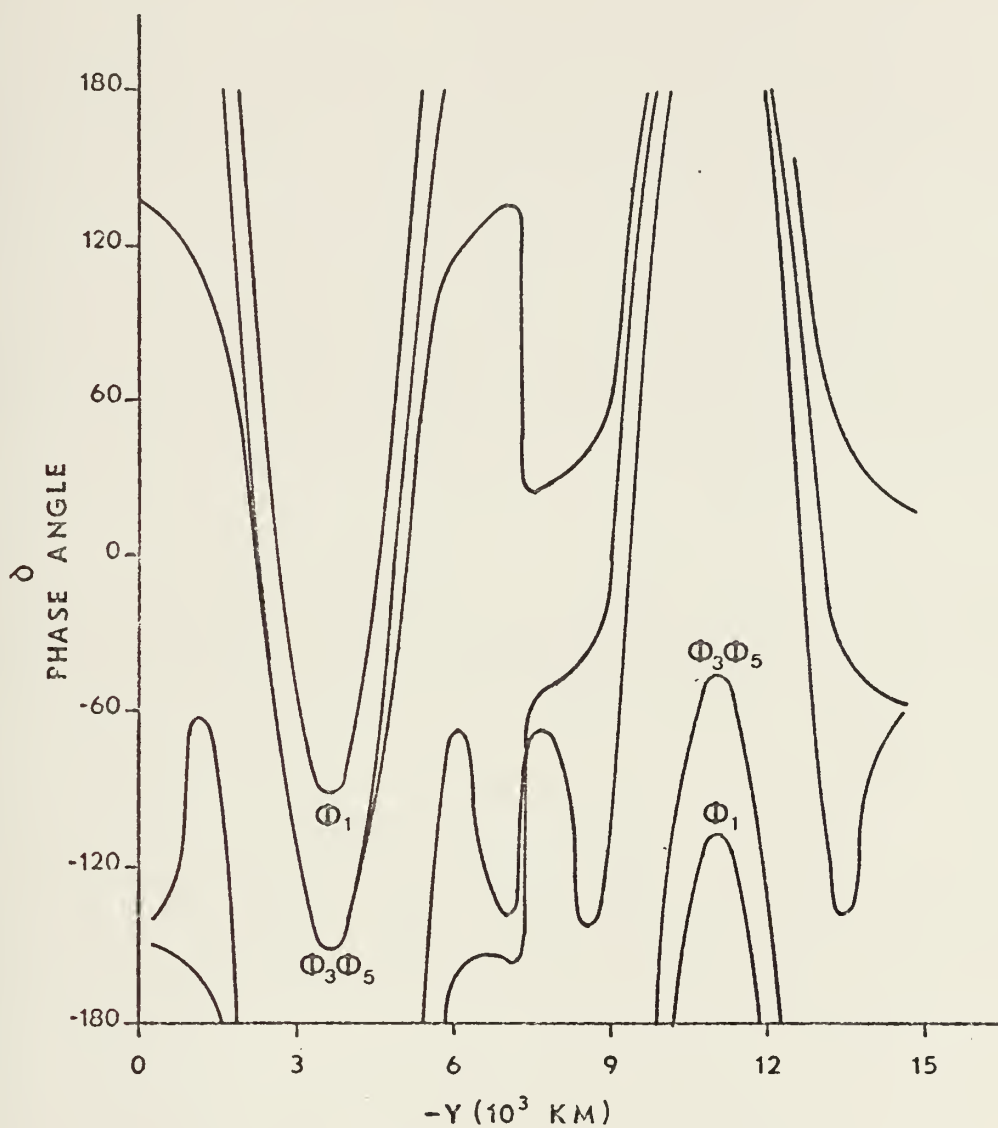


FIGURE 15 - Phase Angles of ϕ_1 , ϕ_3 , and ϕ_5 as a Function of Y for $\Delta P = 50$ CB, $P = 5000$ CB, $R_L = 75$ KM, and x -wavelength of 600 KM.

of the Rossby deformation length. The phase angles for each level showed that all of the waves were barotropically stable, since the phase lag in y was in the same sense as the horizontal wind shear. Also, the vertical tilt was in the opposite sense to the vertical shear as is to be expected for baroclinic instability. Note that the y -scale of the disturbance is much smaller for $R_L = 75$ KM compared to $R_L = 750$ KM. This result was predicted by Stone (1969) who showed that in a slowly varying wind field the y -scale of baroclinic waves would be of the order of the Rossby deformation length. It was observed that the amplitude in the disturbance fields for $R_L = 75$ KM was contained in two narrow regions centered about 2600 KM and 7500 KM.

Friction and heating were added to the model in the second experiment to study the nonlinear effects. The equilibrium temperature profile $\frac{\partial \phi^*}{\partial p}$ was obtained from the initial value of $\frac{\partial \phi}{\partial p}$. This has the effect of maintaining the mean wind, since the heating will tend to restore the mean temperature field to its initial conditions when the disturbance amplitude is sufficient to cause a departure. Heating was present in the mean field only. The radiative time constant τ was 10 Jupiter days. The friction term was present in all fields. The friction coefficient B was equal to 1.0×10^5 and 5.0×10^5 for Rossby deformation lengths of 750 KM and 75 KM, respectively. Since the grid mesh distance was 150 KM and the x -wavelength was 600 KM, the grid may have difficulty resolving the wave;

therefore, a larger value of the friction coefficient was needed to maintain stability in the model. The mean field was allowed full interaction with the disturbance fields. Two cases corresponding to the Rossby deformation lengths were performed with a lower layer thickness of 500 CB. All other initial conditions were as described in the linear experiment.

The model was integrated for 10^4 Jupiter days with a Rossby deformation length of 75 KM. At this time the model became unstable. The corresponding mean zonal wind profile and disturbance amplitudes and phase relationships are shown in Figures 16 through 18. The maximum wind speeds were 25.9 meters per second for the northern easterlies and 26.3 meters per second for the southern westerlies. Zonal velocities also developed in layers 3 and 5. The relative minima associated with the maximum wind is the result of the amplitude of the disturbance fields. These amplitudes are similar to the linear case except the peaks are now bimodal and the profile has a broader base, indicating the disturbance energy has been distributed over a larger region. The phase angles showed baroclinic instability in the vicinity of the maximum mean zonal wind in the north and the south, since the sense of the vertical wind shear was opposite the tilt of the phase.

Because the 750 KM Rossby deformation length case has a much slower disturbance growth rate, the experiment was run for 536 Jupiter days. The mean zonal wind profile is

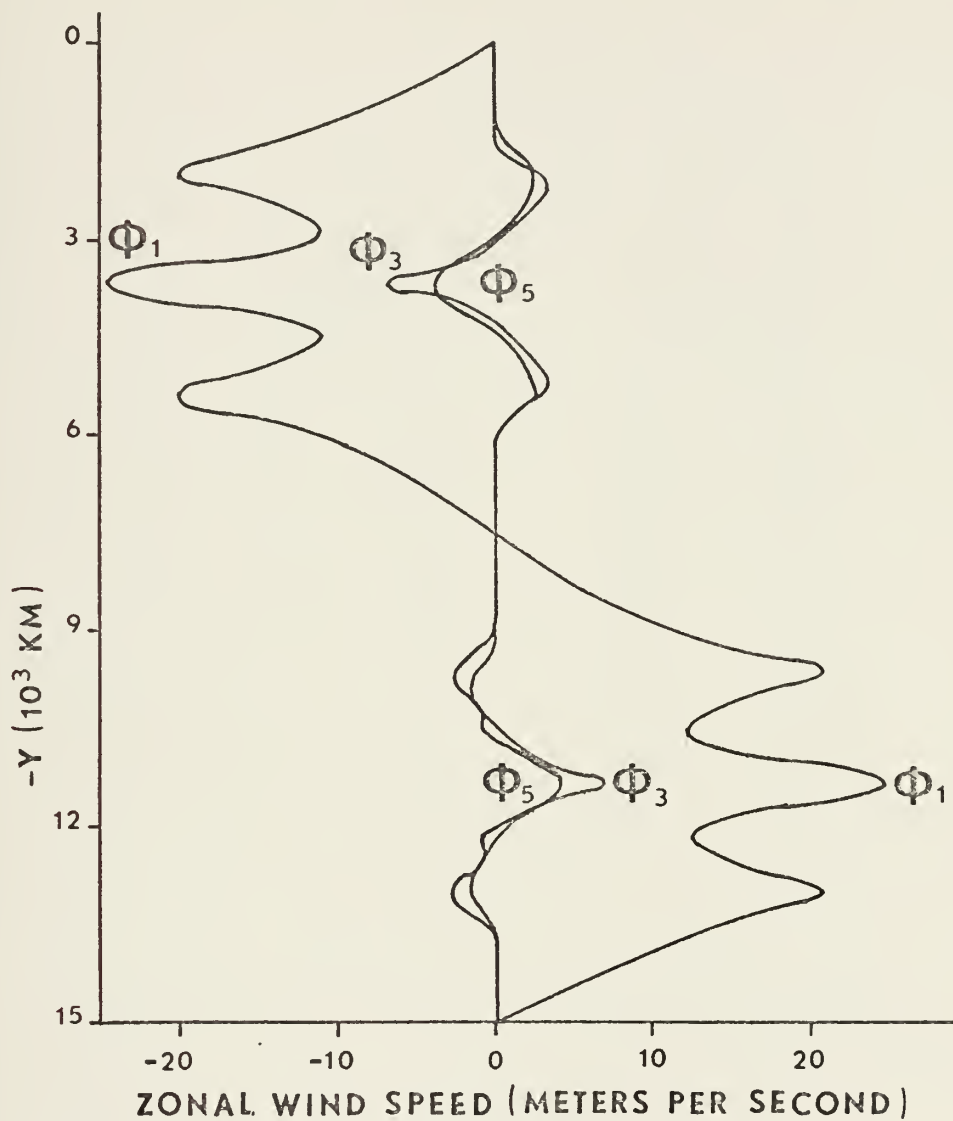


FIGURE 16 - Mean Zonal Wind for $\Delta P = 50$ CB,
 $P = 500$ CB, $R_L = 75$ KM, and
 x-wavelength of 600 KM for
 Jupiter Day 104.

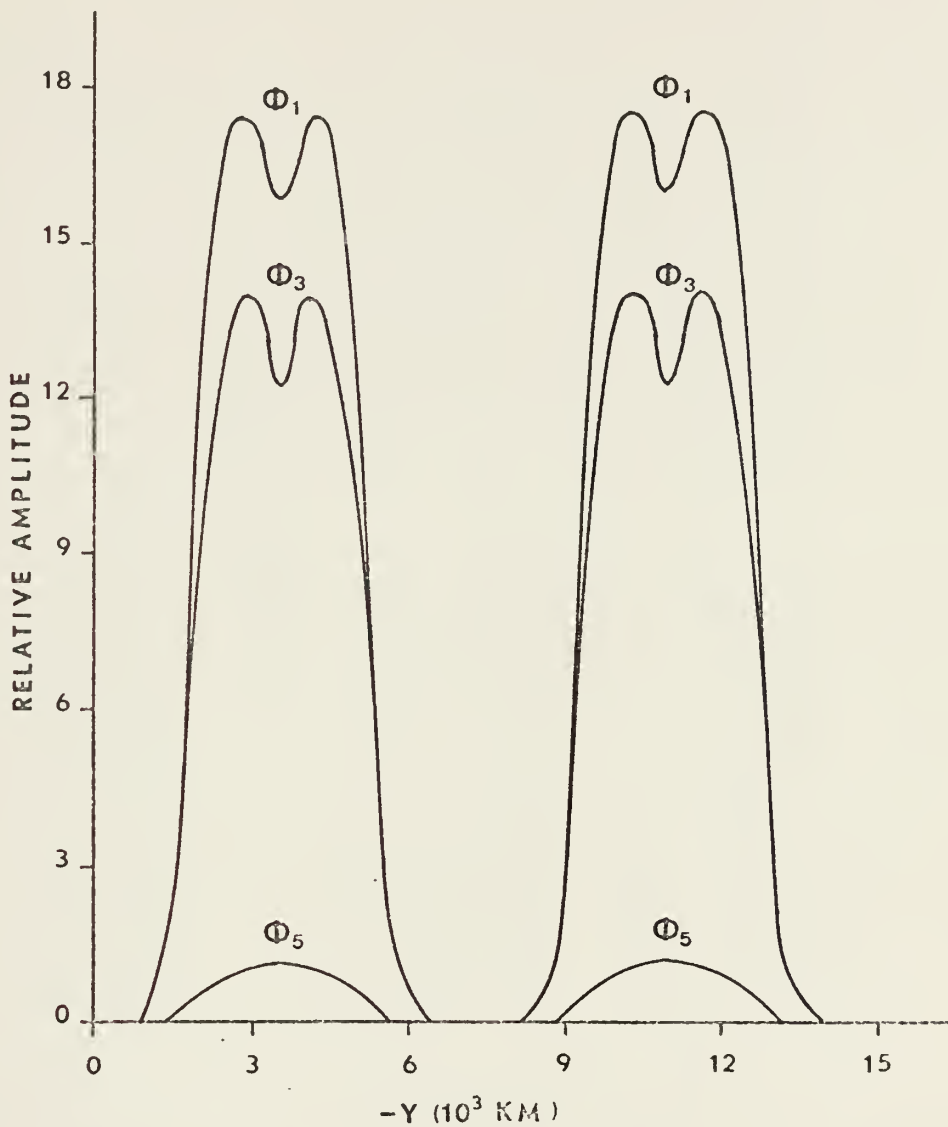


FIGURE 17 - Relative Amplitude of ϕ_1 , ϕ_3 , and ϕ_5 as a Function of Y for $\Delta P = 50$ CB, $P = 500$ CB, $R_L = 75$ KM, and x -wavelength of 600 KM for Jupiter Day 104.

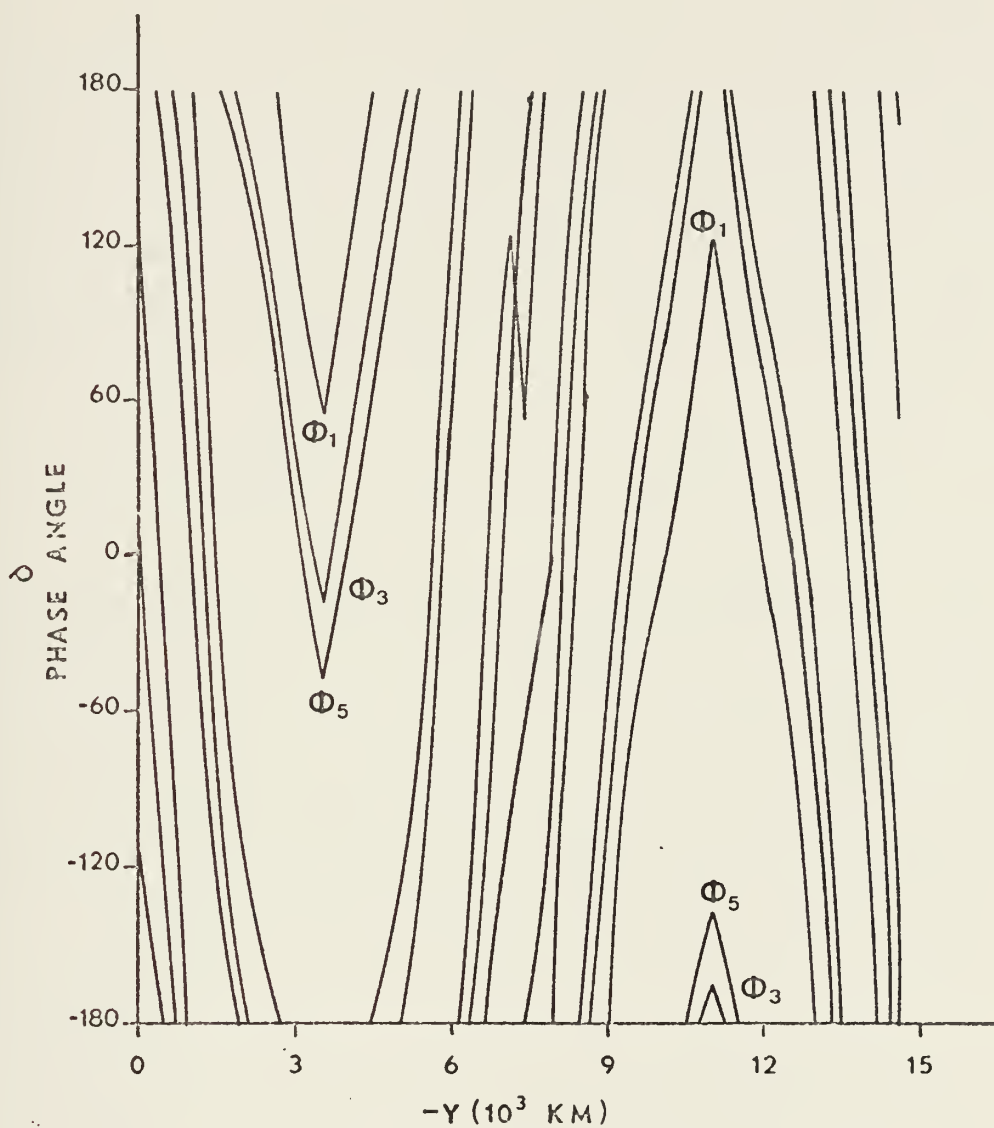


FIGURE 18 - Phase Angles of ϕ_1 , ϕ_3 , and ϕ_5 as a Function of Y for $\Delta P = 50$ CB, $P = 500$ CB, $R_L = 75$ KM, and x-wavelength of 600 KM for Jupiter Day 104.

shown in Figure 22. Relatively small changes have occurred compared with the other nonlinear case. The mean wind speed is 20.7 meters per second in level 1. Small amplitude winds have developed in levels 3 and 5; however, no appreciable wind is observed in level 5 in the south. Figure 21 shows the amplitude of the most unstable wave in the disturbance field as a function of time. The growth rate is exponential with value

$$\frac{1}{A} \frac{\partial A}{\partial t} = 0.21 \times 10^{-6} \text{ sec}^{-1}$$

thus the field has not reached quasi-equilibrium. The disturbance amplitudes shown in Figure 19 indicate the effects of the planetary vorticity gradient β have been reduced. The northern disturbance has a relatively greater amplitude in all three levels. The relative amplitude of ϕ_s is an order of magnitude smaller as observed in the linear case.

One inconsistency was present in this experiment which has not been resolved. The growth rates observed in the linear mode were an order of magnitude larger than the nonlinear mode. This was not a physical result, but an error in the program.

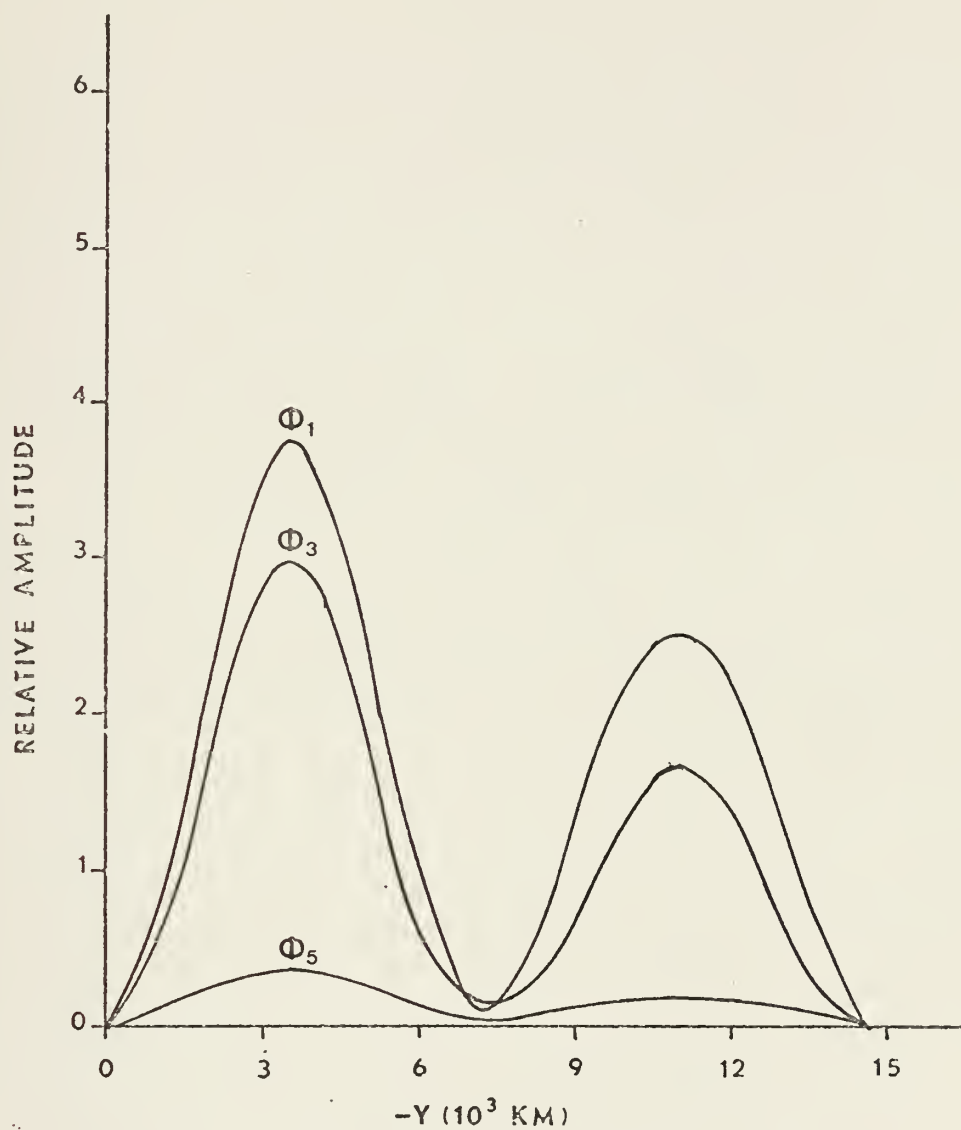


FIGURE 19 - Relative Amplitude of ϕ_1 , ϕ_3 , and ϕ_5 as a Function of Y for $\Delta P = 50$ CB, $P = 500$ CB, $R_L = 750$ KM, and x-wavelength of 6000 KM for Jupiter Day 536.

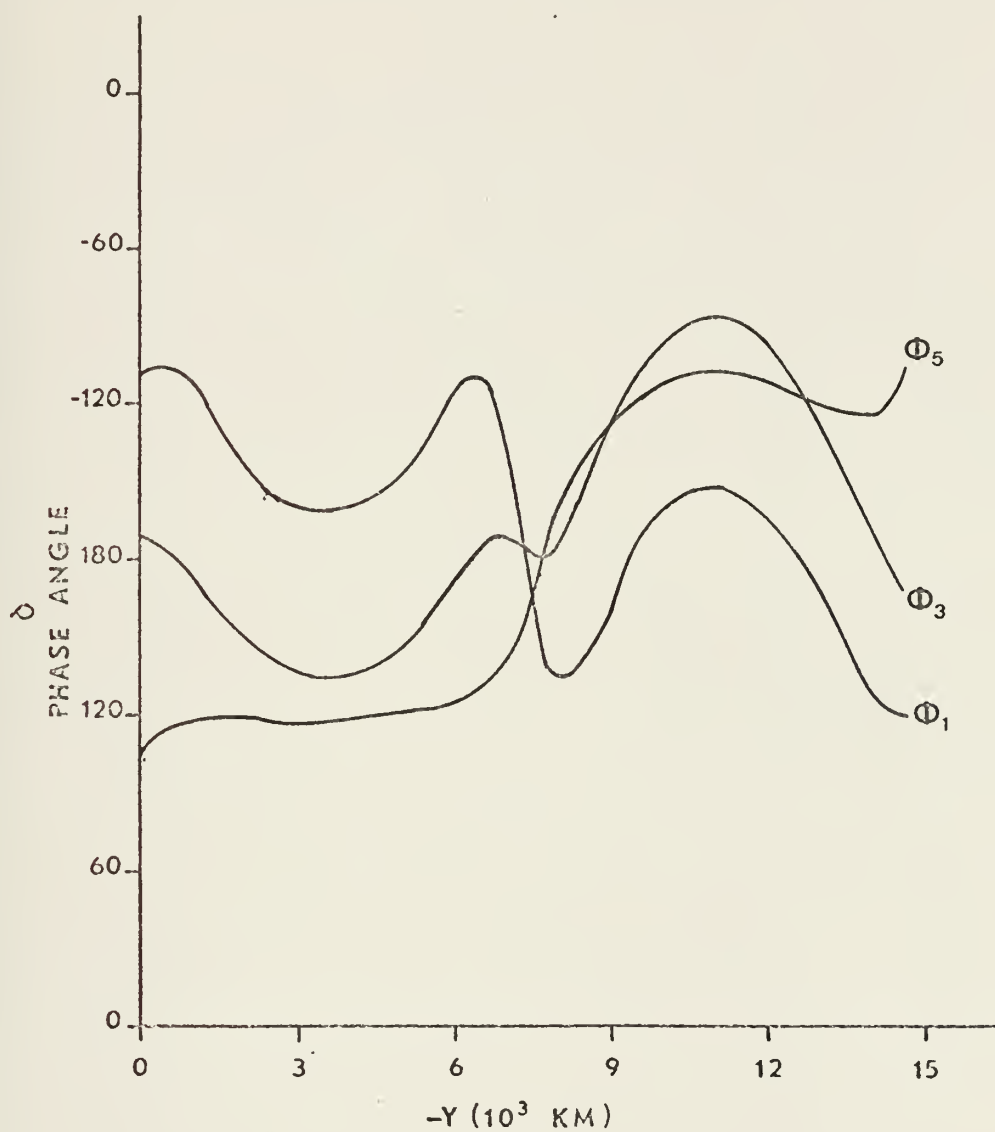


FIGURE 20 - Phase Angles of ϕ_1 , ϕ_3 , and ϕ_5 as a Function of Y for $\Delta P = 50$ CB, $P = 500$ CB, $R_L = 750$ KM, and x-wavelength of 6000 KM for Jupiter Day 536.

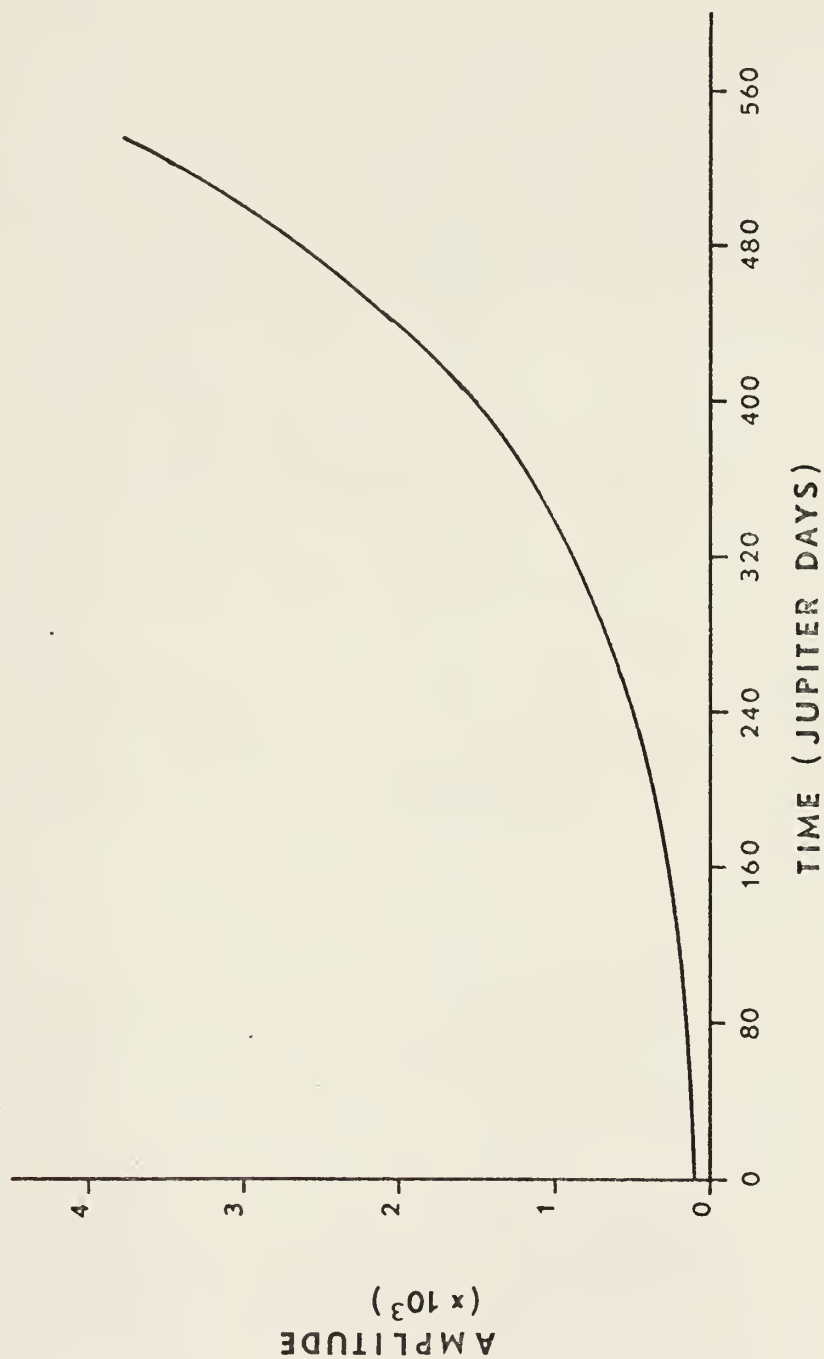


FIGURE 21 - Amplitude of Y-Disturbance Versus Time for
 $\Delta P = 50$ CB, $P = 500$ CB, $R_L = 750$ KM, and
 x-wavelength of 6000 KM.

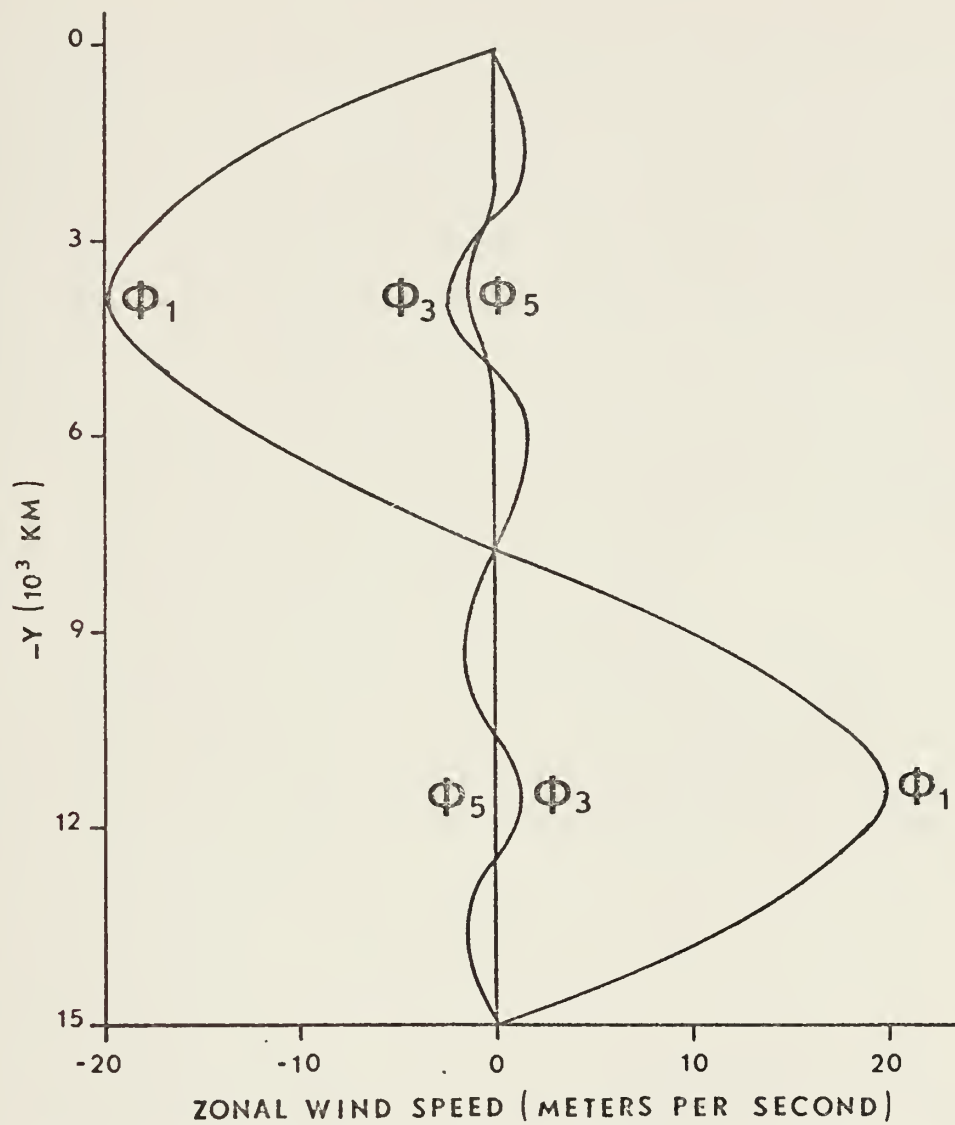


FIGURE 22 - Mean Zonal Wind for $\Delta P = 50$ CB,
 $P = 500$ CB, $R_L = 75$ KM, and
 x-wavelength of 600 KM for
 Jupiter Day 536.

IV. CONCLUSIONS

A three-level quasi-geostrophic atmospheric model has been examined on a β -plane with a single wave in the x-direction and a deep lower layer of varying thickness. The disturbance structure in y was investigated to determine the linear interactions with a constant mean wind and for nonlinear interactions with a varying mean wind. Simple heating to maintain the mean wind and friction were included in the nonlinear case. Two values of the Rossby deformation length were included in the experiments.

The linear experiment showed that the growth rates in the disturbance field are largely independent of the lower layer depth (Figure 2). These growth rates are a function of the Rossby deformation length and the x-wavelength. The waves were barotropically damped in this case, since the relative vorticity gradient was less than or equal to the planetary vorticity gradient. This was obvious since the phase tilt was in the same sense as the horizontal wind shear.

The heating function was not important in the nonlinear experiment, since the model never reached a long term steady state. The disturbance fields were barotropically damped. In the cases studied the zonal disturbances are baroclinically unstable. If the actual wind structure on Jupiter is baroclinically stable as suggested by Ingersoll and Cuzzi (1969),

then this could be accomplished by distributing the mean change through great depth. This would give a very small shear which could be stabilized by β . The growth rates were expected to decrease with increasing lower layer depths, but in fact they did not. Thus it may be that the lower layer was not properly formulated by this model.

Further investigation of the disturbance growth rates is required to resolve the discrepancy between the linear and nonlinear cases. It is also recommended that the grid mesh be reduced to more realistically model the 600 KM x-wavelength. This should allow use of a smaller friction coefficient.

APPENDIX

GEOPHYSICAL AND ASTRONOMICAL CONSTANTS OF JUPITER AND EARTH

PARAMETER	JUPITER	EARTH
Perihelion Distance, A.U. ⁸ (1 A.U. = 1.496×10^8 KM)	4.951	0.9833
Amphelion Distance, A.U.	5.455	1.0167
Siderial Period, (day)	10,759.20	365.256
Inclination of orbit to ecliptic	3°04'	23°27'
Mass, (GM)	1.899×10^{30}	5.976×10^{27}
Density, (GM/CM ³)	1.33	5.517
Mean Radius, (KM)	69,828	6,371
Equatorial Gravitational Acceleration, (CM/SEC ²)	2587	979
Albedo	0.73	0.36
Orbital Eccentricity	0.0483	0.01627
Mean Temperature	130° K	330° K
Solar Constant, (Ly,MIN)	~0.07	~2
Ω , (SEC ⁻¹)	17.6×10^{-5}	7.3×10^{-5}
Observed Mean Wind, (M/SEC)	50	15
Rossby Number, R_o	0.0041	0.032
Rossby deformation Length, (KM)	785, 78.5	1,000

PARAMETER	JUPITER	EARTH
Coriolis Parameter, (45°)	$2.5 \times 10^{-4} \text{ SEC}^{-1}$	$1.0 \times 10^{-4} \text{ SEC}^{-1}$
Planetary Vorticity Gradient, (45°), ($\text{SEC}^{-1} \text{M}^{-1}$)	3.6×10^{-12}	1.6×10^{-11}
R_L/a	0.05	0.63

LIST OF REFERENCES

1. Charney, J. G. and Phillips, N. A., 1953: "Numerical Integration of the Quasi-geostrophic Equations for Barotropic and Simple Baroclinic Flows," Journal of Meteorology, 10,2,71-99.
2. Gierasch, P. J., 1973: "Jupiter's Banded Structure," Submitted for publication.
3. Gierasch, P. J., Ingersoll, A. P., and Williams, R. T., 1973: "Radiative Instability of a Cloudy Planetary Atmosphere," Submitted for publication.
4. Ingersoll, A. P. and Cuzzi, J. N., 1969: "Dynamics of Jupiter's Cloud Bands," Journal of the Atmospheric Sciences, 26,5, 979-985.
5. Lewis, J. S., 1969: "The Clouds of Jupiter and the $\text{NH}_3\text{-H}_2\text{O}$ and $\text{NH}_3\text{-H}_2\text{S}$ Systems," Icarus, 10, 365-378.
6. Lorenz, E. N., 1960: "Maximum Simplification of the Dynamic Equations," Tellus, 12,3, 243-254.
7. Matsuno, J., 1966: "Numerical Integration of the Primitive Equations by a Simulated Backward Difference Method," Journal of the Meteorological Society of Japan, Ser 2, 44, 76-84.
8. Peek, B. M., 1958: "The Planet Jupiter," London, Faber and Faber, 283 pp.
9. Stone, P. H., 1966a: "On Non-geostrophic Baroclinic Stability," Journal of the Atmospheric Sciences, 23, 390-400.
10. Stone, P. H., 1966b: "The Meridional Structure of Baroclinic Waves," Journal of the Atmospheric Sciences, 26,3, 376-389.
11. Stone, P. H., 1967: "An Application of Baroclinic Stability Theory to the Dynamics of the Jovian Atmosphere," Journal of the Atmospheric Sciences, 24,6, 642-652.

12. Stone, P. H., 1972: "A Simplified Radiative-dynamical Model for the Static Stability of Rotating Atmospheres," Journal of the Atmospheric Sciences, 29, 405-418.
13. Richtmeyer, R. D., 1957: "Difference Methods for Initial Value Problems," Interscience Publications, Inc., New York.

INITIAL DISTRIBUTION LIST

	No. Copies
1. Defense Documentation Center Cameron Station Alexandria, Virginia 22314	2
2. Library, Code 0212 Naval Postgraduate School Monterey, California 93940	2
3. Professor R. T. Williams, Code 51Wu Department of Meteorology Naval Postgraduate School Monterey, California 93940	10
4. Navy Weather Service Command Washington Navy Yard Washington, D. C. 20390	1
5. Officer in Charge Environmental Prediction Research Facility Naval Postgraduate School Monterey, California 93940	1
6. Commanding Officer U. S. Fleet Weather Central COMNAVMARIANAS, Box 12 FPO San Francisco, California 96630	1
7. Commanding Officer Fleet Numerical Weather Central Naval Postgraduate School Monterey, California 93940	1
8. AFCRL - Research Library L. G. Hanscom Field Attn: Nancy Davis/Stop 29 Bedford, Massachusetts 01730	1
9. Director, Naval Research Laboratory Attn: Tech. Services Info. Officer Washington, D. C. 20390	1
10. Department of Meteorology Code 51 Naval Postgraduate School Monterey, California 93940	3

11. Department of Oceanography 1
Code 58
Naval Postgraduate School
Monterey, California 93940
12. American Meteorological Society 1
45 Beacon Street
Boston, Massachusetts 02128
13. Office of Naval Research 1
Department of the Navy
Washington, D. C. 20360
14. Atmospheric Sciences Library 1
National Oceanic and Atmospheric
Administration
Silver Spring, Maryland 20910
15. Professor Victor Starr 1
Department of Meteorology
M. I. T.
Cambridge, Massachusetts 03139
16. Dr. J. Pedlosky 1
Department of Geophysical Sciences
University of Chicago
Chicago, Illinois 60637
17. National Center for Atmospheric Research 1
Box 1470
Boulder, Colorado 80302
18. Dr. J. Smagorinsky 1
Director
Geophysical Fluid Dynamics Laboratory
Princeton University
Princeton, New Jersey 08540
19. Professor N. A. Phillips 1
Department of Meteorology
M. I. T.
Cambridge, Massachusetts 02139
20. Professor J. G. Charney 1
54-1424
M. I. T.
Cambridge, Massachusetts 02139
21. Dr. A. Arakawa 1
Department of Meteorology
UCLA
Los Angeles, California 90024

- | | | |
|-----|-------------------------------------------------------------------------------------------------------------------|---|
| 22. | Dr. G. Haltiner
Chairman, Department of Meteorology
Naval Postgraduate School
Monterey, California 93940 | 1 |
| 23. | Dr. R. Haney
Department of Meteorology
Naval Postgraduate School
Monterey, California 93940 | 1 |
| 24. | Dr. R. Elsberry
Department of Meteorology
Naval Postgraduate School
Monterey, California 93940 | 1 |
| 25. | Dr. C. P. Chang
Department of Meteorology
Naval Postgraduate School
Monterey, California 93940 | 1 |
| 26. | Dr. J. Galt
Department of Oceanography
Naval Postgraduate School
Monterey, California 93940 | 1 |
| 27. | Dr. K. Davidson
Department of Meteorology
Naval Postgraduate School
Monterey, California 93940 | 1 |
| 28. | Dr. R. Alberty
National Severe Storms Laboratory
1313 Halley Circle
Normal Oklahoma 73069 | 1 |
| 29. | Professor Peter J. Gierasch
Space Sciences Building
Cornell University
Ithaca, New York 14850 | 1 |
| 30. | Dr. Peter H. Stone
Institute for Space Studies
2880 Broadway
New York, New York 10025 | 1 |
| 31. | Dr. S. Piacsek
Code 7750
Naval Research Lab
Washington, D. C. 20390 | 1 |

32. Dr. A. P. Ingersoll 1
Division of Geological and Planetary
Sciences
California Institute of Technology
Pasadena, California 91109
33. Mrs. O. Haney 1
Environmental Prediction Research Facility
Naval Postgraduate School
Monterey, California 93940
34. Dr. J. Holton 1
Department of Atmospheric Sciences
University of Washington
Seattle, Washington 98105
35. Dr. J. Young 1
Department of Meteorology
University of Wisconsin
Madison, Wisconsin 53706
36. Dr. T. Ogura 1
Laboratory for Atmospheric Research
University of Illinois
Urbana, Illinois 61801
37. Dr. J. Mahlman 1
Geophysical Fluid Dynamics Laboratory
Princeton University
Princeton, New Jersey 08540
38. Dr. R. Alexander 1
The Rand Corporation
1700 Main Street
Santa Monica, California 90406
39. Dr. W. L. Gates 1
The Rand Corporation
1700 Main Street
Santa Monica, California 90406
40. Dr. Conway Leary 1
Dept. of Atmospheric Sciences
University of Washington
Seattle, Washington 98105
41. Dr. W. Van Der Bijl 1
Department of Meteorology
Naval Postgraduate School
Monterey, California 93940

42. Lieutenant Francis Rust Wooldridge
U.S. NWSED Misawa
APO San Francisco, Calif. 96519

5

DOCUMENT CONTROL DATA - R & D

(Security classification of title, body of abstract and indexing annotation must be entered when the overall report is classified)

ORIGINATING ACTIVITY (Corporate author)

Naval Postgraduate School
Monterey, California 93940

2a. REPORT SECURITY CLASSIFICATION

Unclassified

2b. GROUP

REPORT TITLE

General Circulation of Jupiter's Atmosphere

DESCRIPTIVE NOTES (Type of report and, inclusive dates)

Master's Thesis: March 1973

AUTHOR(S) (First name, middle initial, last name)

Francis Rust Wooldridge

REPORT DATE

March 1973

7a. TOTAL NO. OF PAGES

63

7b. NO. OF REFS

13

CONTRACT OR GRANT NO.

9a. ORIGINATOR'S REPORT NUMBER(S)

PROJECT NO.

9b. OTHER REPORT NO(S) (Any other numbers that may be assigned this report)

DISTRIBUTION STATEMENT

Approved for public release; distribution unlimited.

SUPPLEMENTARY NOTES

12. SPONSORING MILITARY ACTIVITY

Naval Postgraduate School
Monterey, California 93940

ABSTRACT

A three-level quasi-geostrophic atmospheric model on a mid-atmosphere β -plane with a single wave in the x-direction and a thick lower layer was developed. This model was used to determine the disturbance structure in y for linear interactions with a constant mean wind and nonlinear interactions with a varying mean wind. Simple heating to maintain the mean wind and friction were included in the nonlinear case.

The linear experiment produced exponential growth rates in the disturbance field that were independent of the lower layer thickness. These waves were baroclinically unstable. The mean wind field showed large modifications for a Rossby deformation length of 75 KM at 10⁴ Jupiter days.

KEY WORDS

LINK A

LINK B

LINK C

ROLE

WT

ROLE

WT

ROLE

W T

quasi-geostrophic model

potential vorticity equations

numerical integration

three-level model

y-disturbance structure

atmospheric general circulation

cloud bands of Jupiter

barotropic stability

baroclinic instability

disturbance growth rates

linear interactions

nonlinear interactions

Rossby deformation length

Jupiter

atmosphere of Jupiter

20 SEP 76

24295

Thesis

W8437 Wooldridge

c.1

General circulation of
Jupiter's atmosphere.

143995

20 SEP 76

24295

Thesis

W8437 Wooldridge

c.1

General circulation of
Jupiter's atmosphere.

143995

thesW8437

General circulation of Jupiter's atmosph



3 2768 001 90625 8

DUDLEY KNOX LIBRARY